In search of the oldest rock of Austria: The Hauergraben Gneiss, a 1.40 Ga old mafic quartz-monzonitic inlayer in the Dobra Gneiss (Drosendorf Unit, Bohemian Massif) as a new candidate

Martin Lindner[1]*, Wolfgang Dörr[2], Christoph A. Hauzenberger[3], Daniel Reither[4], Fritz Finger[5]

[1] Department of Chemistry and Physics of Materials, University of Salzburg, Jakob-Haringer-Straße 2a, 5020 Salzburg, Austria; corresponding author, lindnerma55@gmail.com, Orcid ID 0000-0002-5147-6303

[2] Institut für Geowissenschaften, Goethe-Universität, FE Geologie, Altenhöferallee 1, 60438 Frankfurt am Main, Germany; w.doerr@em.uni-frankfurt.de

[3] NAWI Graz Geocenter – Institute of Earth Sciences, University of Graz, Universitaetsplatz 2, Graz 8010, Austria; christoph.hauzenberger@uni-graz.at

[4] Department of Geography and Geology, University of Salzburg, Hellbrunnerstraße 34, 5020 Salzburg, Austria; mcreither@gmail.com

[5] Department of Geography and Geology, University of Salzburg, Hellbrunnerstraße 34, 5020 Salzburg, Austria and NAWI Graz Geocenter – Institute of Earth Sciences, University of Graz, Universitaetsplatz 2, Graz 8010, Austria; Friedrich.Finger@sbg.ac.at

*) Corresponding author: Martin Lindner

Abstract

For a long time, the 1.38 Ga old Dobra Gneiss (Type A) from the Lower Austrian Drosendorf Unit (Moldanubian Zone, Bohemian Massif) was considered the oldest rock of Austria. We now have dated zircons from a local mafic inlayer in the Dobra Gneiss Type A, termed Hauergraben Gneiss. This small-scale amphibole-bearing orthogneiss has a magmatic formation age of 1.40 Ga, and is, thus, to the present state of knowledge, the oldest rock of Austria. Based on geochemical investigations, the protolith of the Hauergraben Gneiss was a quartz-monzonite. It probably originated in a volcanic arc setting like the Dobra Gneiss, but shows distinctively higher transitional metal contents (especially Cr and Co), higher Ba and Sr, and higher light rare earth element contents, which hint at a lithospheric mantle input. This 1.40 Ga old mafic arc material was then incorporated into the 1.38 Ga old intrusive protolith of the Dobra Gneiss, probably in the form of enclaves. Considering the model that the Drosendorf Unit was part of Amazonia until the late Neoproterozoic, we propose that both, Dobra Gneiss Type A and Hauergraben Gneiss, originated at the western margin of the Columbia supercontinent, where several long-lived Mesoproterozoic volcanic arcs existed and accreted over time. During the Variscan orogeny, the Hauergraben Gneiss experienced peak metamorphic temperatures of ~620 °C at pressures of ~6 kbar, as can be deduced from amphibole thermobarometry. This is in line with published peak-PT estimates from other parts of the Drosendorf Unit. Formation of secondary low-Al magnesiohornblende at the expense of the earlier edenitic/pargasitic peak amphibole indicates a subsequent retrograde overprint.

Kurzfassung

Lange Zeit galt der auf 1.38 Ga datierte Dobra Gneis (Typ A) aus der niederösterreichischen Drosendorf Einheit (Moldanubische Zone, Böhmische Masse) als das älteste Gestein Österreichs. In dieser Arbeit präsentieren wir neue U-Pb Datierungen an Zirkonen aus einer mafischen Einlagerung im Dobra Gneis Typ A, dem sogenannten Hauergraben Gneis. Dabei handelt es sich um einen gering verbreiteten, amphibolhaltigen Orthogneis mit quarz-monzonitischer Zusammensetzung, welcher mit einem magmatischen Bildungsalter von 1.40 Ga, nach derzeitigem Kenntnisstand, das älteste Gestein Österreichs darstellt. Basierend auf geochemischen Untersuchungen kann das magmatische Edukt des Hauergraben Gneises einem Vulkanbogen zugeschrieben werden, wie auch der etwas jüngere Dobra Gneis Typ A. Im Gegensatz zu letzterem besitzt der Hauergraben Gneis jedoch höhere Gehalte an Übergangsmetallen (vor allem Cr und Co), Ba, Sr und den leichten Seltenen Erden. Dies deutet auf eine lithosphärische Mantelquelle hin. Der 1.40 Ga alte Hauergraben Gneis wurde anschließend vom plutonischen Edukt des Dobra Gneis Typ A vermutlich in Schollenform aufgenommen. Der Modellvorstellung folgend, dass die Drosendorf Einheit bis ins späte Neoproterozoikum Teil des Amazonas Kratons war, nehmen wir als Bildungsort für den Hauergraben Gneis und den Dobra Gneis Typ A die Westseite des Columbia Superkontinents an. Dort entstanden im Mesoproterozoikum mehrere langlebige Vulkanbögen, welche sich nach und nach an den Kontinent anlagerten. Am Höhepunkt der Variszischen Gebirgsbildung erfuhr der Hauergraben Gneis Metamorphose Temperaturen um die 620 °C bei einem Druck von ca. 6 kbar, wie man durch Amphibol Geothermobarometrie ableiten kann. Dies deckt sich mit veröffentlichten PT-Pfaden für andere Teile der Drosendorf Einheit. Die Bildung von sekundären Magnesiohornblenden auf Kosten der älteren Edenite/Pargasite deutet auf eine spätere, retrograde Überprägung hin.

1. Introduction

The Lower Austrian Drosendorf Unit, situated in the south-eastern part of the Moldanubian Zone of the Bohemian Massif, hosts some of the oldest rocks of Austria (Finger and Schubert, 2015). It consists of a variegated series of lithologies, including paragneiss, quartzite, marble, calc-silicate, amphibolite and orthogneiss (Fuchs and Matura, 1976), and was, thus, also termed "Bunte Serie" ("Variegated Series") in earlier work (Waldmann, 1951; Fuchs, 1970, 1971). For the major orthogneiss body in the Drosendorf Unit, the Dobra Gneiss (Fuchs and Matura, 1976), a formation age of 1.38 Ga was reported in a SHRIMP zircon study (Gebauer and Friedl, 1994). An early Neoproterozoic protolith age of 800-900 Ma was inferred for the marbles of the Drosendorf Unit, based on their low 87Sr/86Sr ratios (Frank et al., 1990). The Spitz orthogneiss (Fuchs and Matura, 1976; Lindner and Finger, 2018) yielded a U-Pb zircon age of 614 Ma (Friedl et al., 2004). Potentially younger rocks are the amphibolites of the Drosendorf Unit, which were interpreted by Finger and Steyrer (1995) as Early Palaeozoic rift basalts. Some of these amphibolites may even be Devonian in age (Friedl, 1997). The whole Drosendorf Unit received a medium to high grade metamorphic overprint during the Variscan orogeny (Sorger et al., 2020). Consequently, it includes a geological record that spans at least a billion years.

The use of LA-ICP-MS zircon dating provides a powerful means to further resolve the geological evolution of the Drosendorf Unit. Using this method in combination with a comprehensive geochemical investigation, Lindner et al. (2020) could show that the Dobra Gneiss is only in part a Mesoproterozoic rock (Dobra Gneiss Type A), and that large portions of it (Dobra Gneiss Type B) represent a Cadomian, 570-580 Ma old granitic intrusive rock.

The 1.38 Ga old Dobra Gneiss (strictly speaking the Dobra Gneiss Type A, according to Lindner et al., 2020) is commonly referred to as the oldest rock of Austria (e.g. Meschede, 2015; Schuster et al., 2019). Here we show that rare mafic orthogneiss inlayers in this rock are still approximately 20 Ma older than the Dobra Gneiss Type A. We give a brief petrographic and geochemical description of this newly recognized "oldest rock of Austria" (Hauergraben Gneiss), along with a full documentation of the results of U-Pb zircon dating.

2. Geological Background

2.1 Regional geology

The subdivision of the Bohemian Massif into the Saxothuringian, Moldanubian and Moravo-Silesian zones (Fig. 1 inset) dates back to the works of Kossmat (1927) and Suess (1926). The Moldanubian Zone in the Lower Austrian part of the Bohemian Massif (Fig. 1) can be further subdivided into the Gföhl, Ostrong, and Drosendorf units, which are Variscan tectonic units juxtaposed in the Early Carboniferous (Fuchs and Matura, 1976; Thiele, 1984; Dallmeyer et al., 1992).

The HT-HP metamorphic Gföhl Unit in the hanging wall consists mainly of migmatitic orthogneiss and granulite. These rocks were exhumed fast and reequilibrated at mid-crustal *P-T* conditions after their deep subduction during an earlier stage of the Variscan orogeny (O'Brien and Carswell, 1993; Cooke et al., 2000; Faryad et al., 2011; Schantl et al., 2019).

The Ostrong Unit is mainly comprised of a monotonous series of *LP-HT* cordierite-bearing paragneiss (Fuchs, 1976; Linner, 1992). Few intercalations of orthogneiss (René and Finger, 2016) and rare relics of eclogite (O'Brien and Vrána, 1995; Scott et al., 2013) are present as well.

Sandwiched between the previously mentioned units is the Drosendorf Unit (Fritz and Neubauer, 1993). It consists of metasedimentary rocks (paragneiss, marble, quartzite, calc-silicate, graphite schist), orthogneiss and amphibolites (Fuchs and Matura, 1976). The orthogneiss parts represent mainly Cadomian granitoids (Spitz Gneiss, Dobra Gneiss Type B; Friedl et al., 2004; Lindner et al., 2020). The internationally renowned Mesoproterozoic Dobra Gneiss Type A forms only some relatively thin, elongated bodies (Fig. 1).

The Moravian Zone in the East (Fig. 1) was overthrust by the Moldanubian nappe pile (incl. the Drosendorf Unit) during the Variscan orogeny, along the so-called main Moldanubian Thrust (Suess, 1926). The Moravian Zone comprises the Cadomian Bittesch Gneiss (Friedl et al., 2000, 2004; Soejono et al., 2017) in the hanging wall, various metasedimentary rocks, and the Late Neoproterozoic granitoid rocks of the Thaya Batholith in the footwall (Finger et al., 1989).

Similarities between the Moravian Bittesch Gneiss and the Moldanubian Dobra Gneiss have already been mentioned by Frasl (1970). Matura (1976, 2003) proposed that both are part of a single, basal Variscan nappe. Lindner et al. (2020) recently provided a geochemical and geochronological study that showed that Dobra Gneiss Type B and Bittesch Gneiss are widely identical rocks. This suggests that the Drosendorf and the Moravian rocks were connected before the Variscan tectonogenesis (see below), and that the main Moldanubian Thrust in the hanging wall of the Bittesch Gneiss is not a terrane boundary.

The granitoids of the South Bohemian Batholith and the Rastenberg Granodiorite pluton (Fig. 1) intruded the the Moldanubian Zone during the waning stages of the Variscan orogeny, between 338 and 300 Ma (Klötzli and Parrish, 1996; Gerdes et al., 2003; Žák et al., 2014)

2.2 Palaeogeographic situation

Many studies (Fuchs, 1971; Matura, 1976; Finger and Steyrer, 1995; Matura, 2003; Lindner and Finger, 2018; Lindner et al., 2020) correlate the Drosendorf and the Moravian rocks with the Brunovistulian terrane (Dudek, 1980; Finger et al., 2000) and the Avalonian margin of the Devonian Old Red continent, respectively (Kroner and Romer, 2013). As can be seen from Figure 2a, most of the Moldanubian Zone (incl. the Gföhl and Ostrong Units in Lower Austria) is thought to belong to a different plate
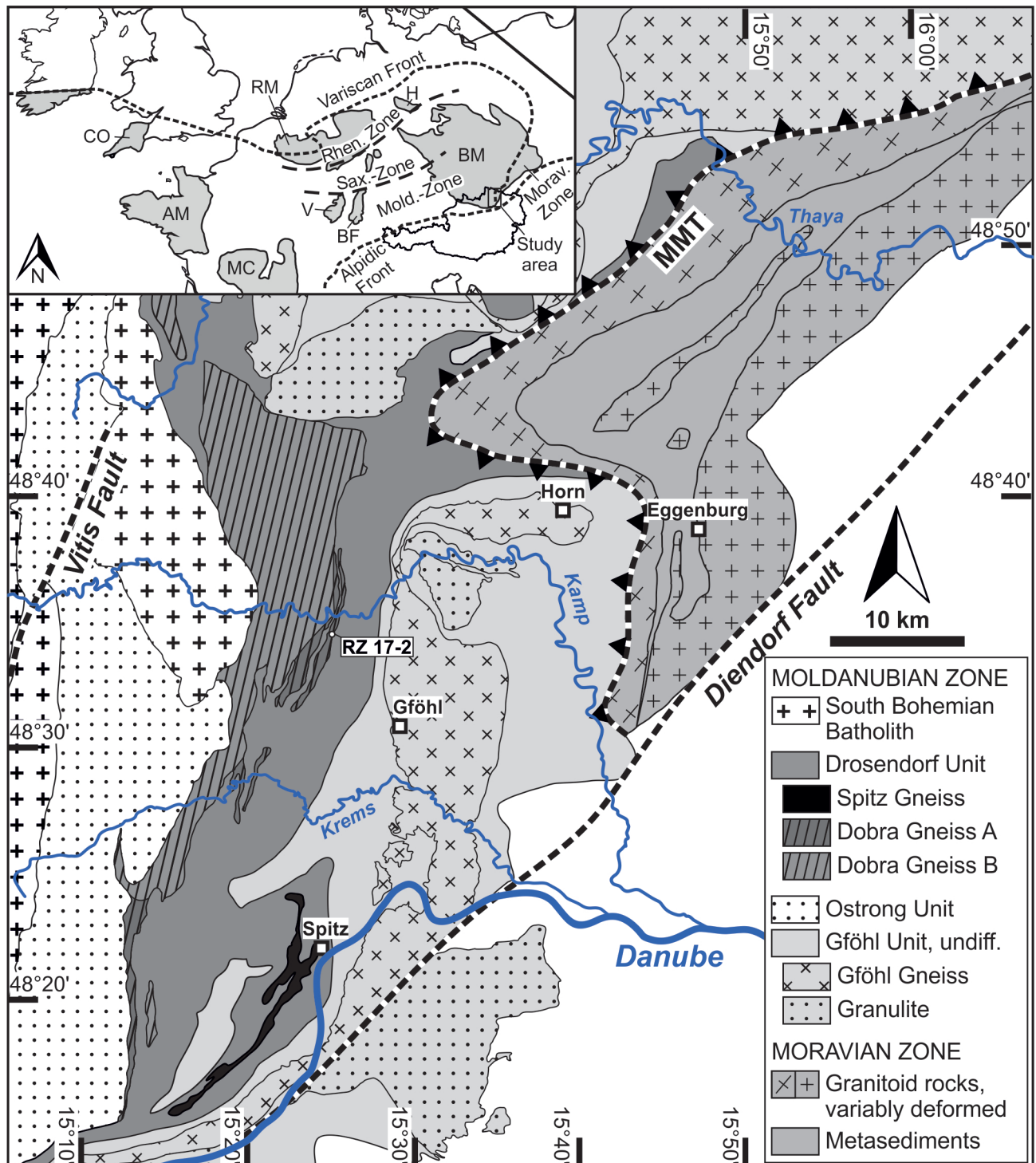
Figure 1: Simplified geological map of the south-eastern Bohemian Massif in Lower Austria with the location of the dated sample of Hauergraben Gneiss. MMT: Main Moldanubian Thrust. Compiled after Fuchs and Matura (1976), Thiele (1984) and Matura (2003). Inset: Variscides in Central Europe. Abbreviations in inset: AM: Armorican Massif; BF: Black Forrest; BM: Bohemian Massif; BV: Brunovistulian (mostly covered); CO: Cornwall; H: Harz; MC: Massif Central; RM: Rhenish Massif; V: Vosges.

tectonic superunit, i.e., the Armorican Terrane Assemblage. The latter was positioned south of the Rheic Ocean before the Variscan orogeny (Tait et al., 1997; Schubert and Finger, 2015). These Armorican rocks show a very distinct Mesoproterozoic gap in their detrital zircon age spectra from ~1.0 to 1.6 Ga (Friedl et al., 2000, 2004; Stephan et al., 2019; Lindner et al., 2020; Sorger et al.,

2020). Conversely, detrital and inherited Mesoproterozoic (i.e. 0.9 – 1.6 Ga old) zircon relics have repeatedly been found in various Brunovistulian rocks (Friedl et al., 2000; Żelaźniewicz et al., 2009, 2020). Due to the presence of Mesoproterozoic zircons, it is commonly assumed that the Brunovistulian terrane (incl. the Moravian and Drosendorf units) was positioned close to the Amazonian

Craton until the late Neoproterozoic, being a part of the western sector of the Avalonian-Cadomian belt of northern Gondwana (Fig. 2b). The North Gondwana ancestry of the Brunovistulian Terrane is generally accepted because of the undisputable Cadomian magmatic record. Lindner et al. (2020) presented a model which describes the rift and drift history of the Brunovistulian terrane from Gondwana to Baltica in the Cambrian (Fig. 2b).

3. Methods

3.1 LA-ICP-MS U-Pb zircon dating
The sample for isotope mass spectrometry was processed at the department of Chemistry and Physics of Materials of the University of Salzburg and at the Institut für Geowissenschaften of the Frankfurt University. Methods included standard mineral separation techniques, including crushing and sieving, concentration of the heavy minerals and magnetic separation with a Frantz isodynamic separator. Zircon grains were mounted in a 25 mm-diameter circular epoxy mount and polished to expose the inner core. Prior to the analysis, the grains were investigated using cathodoluminescence (CL) and back-scattered electron (BSE) imaging to recognize their internal structure and to identify cracks and mineral inclusions. Zircon U–Pb isotope analysis was performed by LA-ICP-MS technique using a Thermo-Finnigan Element II sector field ICPMS attached to a New Wave LUV213 laser ablation system (λ=213 nm) at the Institut für Geowissenschaften, University of Frankfurt. Analytical routines were the same as described in detail in Lindner et al. (2020). Concordia diagrams were generated using IsoplotR (Vermeesch, 2018).

3.2 Whole-rock geochemistry
The samples were analysed for major and selected trace elements using a Bruker Pioneer S4 crystal spectrometer (X-ray fluorescence) at the Department for Chemistry and Physics of Materials, University of Salzburg. The sample preparation and analytical procedure followed standard XRF methods as described in Lindner and Finger (2018). Errors are typically between ±1 to ±3 ppm.

Additionally, one sample was analysed for REE, and Cs, Hf, Ta and U contents at ALS Laboratories in Loughrea, Ireland. The analyses were carried out via ICP-MS on acid digested lithium borate fusion beads. The lower limits of detection are between 0.1 and 0.01 ppm for the above mentioned elements.

3.3 Mineral chemistry
Mineral chemical analyses were performed with a JXA-8530FPlus HyperProbe Electron Probe Microanalyzer (EPMA) at Institute of Earth Sciences - NAWI Graz Geocenter, University of Graz equipped with an energy-dispersive (EDX) and five wavelength-dispersive (WDX) spectrometers. Measurement conditions were 15 kV acceleration voltage, 10 nA beam current and a beam diameter of ~1 - 3 µm. A range of natural and synthetic mineral standards was used for element calibration.

X-ray elemental mapping and additional mineral analyses were performed at the Department of Chemistry and Physics of Materials, University of Salzburg with a ZEISS ULTRAPLUS scanning electron microscope (SEM) and an Oxford X-MAX 50 EDX detector (INCA software). The elemental mapping and EDX analyses were carried out at 25 kV and 3 nA and were calibrated against natural mineral standards (quartz, garnet) as well as synthetic oxides.

4. Results

4.1 Petrography of the Hauergraben Gneiss
The Hauergraben Gneiss is a fine- to medium-grained, weakly foliated mafic rock (Fig. 3a). It is locally found in the area of the Hauergraben, SE of the Dobra dam (Fig. 1) and occurs there in cm- to dm-sized layers within the Dobra Gneiss Type A. The rock is considerably darker than the surrounding Dobra Gneiss and not porphyric. The main mafic mineral is amphibole (~30%). Biotite is mainly found along the foliation plane, but also replaces amphibole (Figs. 3, 4). K-feldspar (~25%), plagioclase (~25%) and quartz (~15%) from an even grained, recrystallized matrix. Accessory minerals are allanite and apatite (abundant), titanite and zircon (Figs. 3, 4). The rock is clearly different from (and should not be confused with) the abundant thin amphibolite intercalations in the Dobra Gneiss, which are largely quartz-free and basaltic in composition. The latter have been interpreted as Early Palaeozoic mafic dykes by Finger and Steyrer (1995).

4.2 Zircon dating
The zircons of sample RZ 17-2 are between 60 and 190 µm long and between 30 and 90 µm wide, with aspect ratios between 1:1 and 4:1. CL imaging shows a diffuse, elongated magmatic zonation in the central parts of the zircons, occasionally also patchy zoning (A192, Fig. 5). No inherited cores are visible (Fig. 5). Most grains show very thin, highly luminescent and probably metamorphic overgrowth rims, which are too small to be targeted with a laser.

A total of 107 spots were analysed. We note a high degree of discordance (Conc% <97) for most of these analyses (Fig. 6, Tab. 1), however, all data points are strictly aligned on a Discordia line with an upper intercept at 1396±3.2 Ma and a lower intercept at 0±5.1 Ma (n=100, MSWD=1.8). Using the most concordant analyses, a Concordia age of 1398±9.7 Ma (n=7, MSWD=0.35) can be calculated. This can be interpreted as the magmatic formation age of the rock. The degree of lead loss is extraordinarily large for some analyses (<50%) and is attributed to recent lead loss. Measuring spots with such a high lead loss were generally located at or close to cracks (e.g. Fig. 5, A186, A138, A139, A221). The well-defined discordia suggests, however, that the measured domains formed all at the same time and remained unaffected by metamorphic recrystallization. On the other hand, the rock is apparently free of pre 1.4 Ga inherited or xenocrystic zircons.

Table 1: U-Pb zircon age data for sample RZ 17-2.

Sample	grain	^{207}Pba (cps)	U^b (ppm)	Pb^b (ppm)	Th U	206 (%)	$\frac{^{206}Pb^d}{^{238}U}$	±2s (%)	$\frac{^{207}Pb^d}{^{235}U}$	±2σ (%)	$\frac{^{207}Pb^d}{^{206}Pb}$	±2s (%)	rho^e	$\frac{^{206}Pb}{^{238}U}$ (Ma)	±2σ (Ma)	$\frac{^{207}Pb}{^{235}U}$ (Ma)	±2σ (Ma)	$\frac{^{207}Pb}{^{206}Pb}$ (Ma)	±2σ (Ma)	conc. (%)
RZ 17-2	A169	221440	995	255	0.65	b.d.	0.237	2.6	2.905	2.7	0.089	0.5	0.98	1373	32	1383	20	1400	10	98
RZ 17-2	A172	211321	922	274	1.35	0.0	0.238	2.8	2.912	2.8	0.089	0.5	0.98	1374	35	1385	22	1403	10	98
RZ 17-2	A192	218743	983	235	0.46	b.d.	0.241	2.9	2.938	2.9	0.088	0.6	0.98	1392	36	1392	22	1391	12	100
RZ 17-2	A204	197727	813	199	0.33	0.1	0.241	2.4	2.954	2.4	0.089	0.6	0.97	1393	30	1396	19	1400	11	100
RZ 17-2	A140	173255	745	177	0.16	1.2	0.242	2.3	2.921	2.7	0.087	1.4	0.85	1399	29	1387	21	1370	28	102
RZ 17-2	A151	121370	551	141	0.60	b.d.	0.244	2.5	3.002	2.6	0.089	0.6	0.97	1407	32	1408	20	1410	12	100
RZ 17-2	A134	168319	501	129	0.33	2.2	0.247	2.5	2.978	4.7	0.088	3.9	0.54	1420	32	1402	36	1374	75	103
RZ 17-2	A210	240229	1170	348	1.63	0.1	0.237	4.6	2.870	4.6	0.088	0.6	0.99	1371	57	1374	35	1380	12	99
RZ 17-2	A153	280058	1153	249	0.04	0.2	0.228	2.3	2.709	2.4	0.086	0.7	0.95	1321	28	1331	18	1347	14	98
RZ 17-2	A166	173667	881	212	0.52	0.2	0.236	3.6	2.884	3.7	0.089	0.6	0.99	1364	44	1378	28	1399	12	97
RZ 17-2	A234	140589	761	175	0.53	0.2	0.228	2.5	2.737	3.4	0.087	2.3	0.74	1325	30	1338	25	1360	43	97
RZ 17-2	A154	179192	728	182	0.48	0.1	0.236	2.4	2.904	2.4	0.089	0.6	0.97	1367	29	1383	19	1408	11	97
RZ 17-2	A160	225469	964	250	0.74	0.0	0.233	2.4	2.860	2.5	0.089	0.6	0.97	1353	29	1371	19	1401	12	97
RZ 17-2	A176	186884	802	196	0.43	0.0	0.235	2.3	2.905	2.4	0.090	0.6	0.96	1363	28	1383	18	1415	12	96
RZ 17-2	A137	138461	642	164	0.68	0.0	0.235	2.3	2.899	2.4	0.089	0.6	0.97	1361	29	1382	18	1414	12	96
RZ 17-2	A193	177942	743	201	0.92	b.d.	0.232	2.4	2.842	2.4	0.089	0.6	0.97	1346	29	1367	19	1399	11	96
RZ 17-2	A203	141882	769	191	0.82	0.2	0.234	3.0	2.890	3.1	0.089	0.6	0.98	1357	37	1379	24	1414	12	96
RZ 17-2	A232	140172	574	164	1.43	b.d.	0.228	2.4	2.772	2.4	0.088	0.6	0.97	1326	29	1348	18	1383	11	96
RZ 17-2	A164	215483	856	210	0.37	0.1	0.235	2.3	2.908	2.4	0.090	0.8	0.94	1361	28	1384	18	1420	15	96
RZ 17-2	A186	111809	515	126	0.69	b.d.	0.232	3.6	2.846	3.6	0.089	0.6	0.99	1345	43	1368	28	1404	12	96
RZ 17-2	A252	114425	617	146	1.04	0.1	0.228	2.5	2.766	4.2	0.088	3.4	0.59	1323	30	1346	32	1384	65	96
RZ 17-2	A162	230101	987	215	0.04	0.1	0.228	2.3	2.779	2.4	0.088	0.6	0.97	1325	27	1350	18	1389	11	95
RZ 17-2	A187	226247	905	259	1.34	0.0	0.230	2.3	2.822	2.4	0.089	0.5	0.98	1334	28	1361	18	1404	10	95
RZ 17-2	A199	127824	562	135	0.30	0.6	0.232	2.3	2.878	3.6	0.090	2.8	0.64	1347	28	1376	27	1421	53	95
RZ 17-2	A231	168244	759	169	0.21	b.d.	0.224	2.4	2.707	2.5	0.088	0.7	0.96	1303	28	1330	18	1375	13	95
RZ 17-2	A170	187510	887	255	1.32	b.d.	0.227	2.7	2.789	2.8	0.089	0.7	0.97	1321	32	1353	21	1403	13	94
RZ 17-2	A185	142028	632	167	0.98	b.d.	0.226	2.3	2.756	2.4	0.089	0.6	0.96	1312	27	1344	18	1394	12	94
RZ 17-2	A243	169696	718	162	0.24	b.d.	0.224	2.3	2.739	2.3	0.089	0.6	0.97	1301	27	1339	18	1401	12	93
RZ 17-2	A173	160460	678	169	0.71	0.5	0.225	2.6	2.777	2.7	0.089	0.8	0.95	1310	31	1349	20	1412	15	93
RZ 17-2	A201	134440	611	145	0.61	0.1	0.220	2.3	2.697	2.4	0.089	0.7	0.96	1281	27	1328	18	1404	13	91
RZ 17-2	A220	95627	429	94	0.16	0.5	0.224	2.3	2.792	2.4	0.090	0.8	0.94	1303	27	1353	18	1434	16	91
RZ 17-2	A214	132811	619	157	0.83	b.d.	0.218	2.3	2.673	2.4	0.089	0.6	0.97	1272	27	1321	18	1401	11	91
RZ 17-2	A215	79301	354	87	0.84	0.3	0.218	2.3	2.689	2.4	0.089	0.8	0.95	1273	27	1325	18	1412	15	90
RZ 17-2	A212	159594	846	204	1.01	b.d.	0.213	2.3	2.592	2.4	0.088	0.6	0.97	1247	26	1298	18	1385	11	90
RZ 17-2	A179	138432	806	176	0.86	2.3	0.202	2.5	2.372	3.7	0.085	2.7	0.68	1186	27	1234	27	1320	53	90
RZ 17-2	A247	126479	570	125	0.38	b.d.	0.213	2.3	2.606	2.3	0.089	0.6	0.96	1245	26	1302	17	1399	12	89
RZ 17-2	A145	154999	752	172	0.60	0.4	0.212	2.4	2.593	2.5	0.089	0.7	0.96	1241	27	1299	19	1395	13	89
RZ 17-2	A218	197029	988	213	0.06	4.4	0.222	2.8	2.821	5.3	0.092	4.5	0.54	1294	33	1361	40	1468	85	88
RZ 17-2	A246	183866	907	188	0.33	b.d.	0.206	3.5	2.502	3.6	0.088	0.5	0.99	1208	39	1273	26	1384	10	87
RZ 17-2	A168	179470	789	165	0.42	b.d.	0.203	2.3	2.446	2.3	0.087	0.6	0.97	1192	25	1256	17	1367	11	87
RZ 17-2	A183	128923	616	145	0.77	0.6	0.203	2.4	2.444	4.4	0.087	3.7	0.54	1191	26	1256	32	1368	71	87
RZ 17-2	A200	192916	838	172	0.16	b.d.	0.208	2.4	2.557	2.4	0.089	0.6	0.97	1218	26	1288	18	1409	12	86
RZ 17-2	A177	169216	820	178	0.46	0.1	0.209	2.5	2.583	2.6	0.090	0.8	0.95	1223	27	1296	19	1418	15	86
RZ 17-2	A190	134783	646	147	0.79	0.1	0.204	2.7	2.484	2.8	0.088	0.7	0.97	1195	30	1267	20	1393	13	86
RZ 17-2	A180	115379	517	119	1.51	1.3	0.205	3.9	2.527	5.0	0.089	3.1	0.78	1203	43	1280	37	1411	60	85
RZ 17-2	A138	165488	746	151	0.30	0.4	0.204	2.4	2.493	2.5	0.089	0.7	0.96	1194	26	1270	18	1400	13	85
RZ 17-2	A175	253276	1144	244	0.51	b.d.	0.202	2.6	2.464	2.7	0.088	0.5	0.98	1187	28	1262	19	1392	10	85
RZ 17-2	A223	156074	819	181	0.96	0.0	0.200	2.9	2.429	3.0	0.088	0.6	0.98	1174	31	1251	22	1387	11	85
RZ 17-2	A224	159104	922	198	0.82	0.2	0.196	2.5	2.374	2.6	0.088	0.6	0.97	1154	27	1235	19	1379	12	84
RZ 17-2	A191	187642	937	203	1.09	b.d.	0.201	2.5	2.482	2.6	0.090	0.7	0.96	1180	27	1267	19	1418	14	83
RZ 17-2	A144	184345	912	191	0.87	0.1	0.195	2.4	2.377	2.5	0.088	0.6	0.97	1148	26	1236	18	1393	11	82
RZ 17-2	A216	263074	1265	234	0.30	b.d.	0.190	2.4	2.299	2.4	0.088	0.5	0.98	1121	24	1212	17	1379	10	81
RZ 17-2	A163	224708	939	195	0.49	0.7	0.192	2.7	2.351	3.4	0.089	2.0	0.81	1132	28	1228	24	1400	37	81
RZ 17-2	A157	208752	985	188	0.52	b.d.	0.189	3.3	2.299	3.4	0.088	0.5	0.99	1116	34	1212	24	1388	10	80

Table 1: U-Pb zircon age data for sample RZ 17-2.

Sample	grain	^{207}Pb^a (cps)	U^b (ppm)	Pb^b (ppm)	Th U	206 (%)	$\frac{^{206}Pb^d}{^{238}U}$	±2s (%)	$\frac{^{207}Pb^d}{^{235}U}$	±2σ (%)	$\frac{^{207}Pb^d}{^{206}Pb}$	±2s (%)	rho^e	$\frac{^{206}Pb}{^{238}U}$ (Ma)	±2σ (Ma)	$\frac{^{207}Pb}{^{235}U}$ (Ma)	±2σ (Ma)	$\frac{^{207}Pb}{^{206}Pb}$ (Ma)	±2σ (Ma)	conc. (%)
RZ 17-2	A237	136863	736	139	0.58	0.9	0.191	2.9	2.345	3.2	0.089	1.3	0.92	1128	30	1226	23	1404	24	80
RZ 17-2	A171	139201	643	156	1.33	b.d.	0.189	2.7	2.303	2.8	0.088	0.6	0.97	1116	28	1213	20	1392	12	80
RZ 17-2	A245	199346	943	177	0.31	b.d.	0.187	2.4	2.271	2.5	0.088	0.6	0.97	1104	24	1203	17	1386	11	80
RZ 17-2	A222	173062	789	171	0.80	0.3	0.189	2.6	2.327	2.7	0.089	1.0	0.93	1117	26	1221	20	1409	19	79
RZ 17-2	A236	130441	571	126	0.76	0.1	0.188	2.8	2.310	2.9	0.089	0.7	0.97	1110	29	1215	21	1408	13	79
RZ 17-2	A230	143553	667	152	1.27	0.2	0.183	2.4	2.239	2.5	0.089	0.6	0.97	1085	24	1193	18	1395	11	78
RZ 17-2	A155	148870	851	167	0.90	0.1	0.181	3.3	2.210	3.3	0.089	0.6	0.98	1071	32	1184	24	1398	12	77
RZ 17-2	A227	79896	393	77	0.73	0.0	0.180	3.2	2.205	3.3	0.089	0.7	0.98	1068	32	1183	23	1400	13	76
RZ 17-2	A178	152008	705	160	1.15	b.d.	0.183	2.4	2.268	2.4	0.090	0.6	0.97	1084	24	1203	17	1423	11	76
RZ 17-2	A228	129812	595	120	0.73	b.d.	0.179	2.9	2.187	3.0	0.089	0.6	0.98	1061	28	1177	21	1397	11	76
RZ 17-2	A209	166852	803	147	0.53	b.d.	0.177	2.3	2.153	2.4	0.088	0.6	0.97	1050	22	1166	17	1388	11	76
RZ 17-2	A152	162679	735	163	1.05	0.6	0.177	2.6	2.161	3.4	0.089	2.2	0.76	1050	25	1168	24	1395	42	75
RZ 17-2	A253	224110	987	177	0.29	0.7	0.173	2.4	2.100	3.2	0.088	2.1	0.75	1030	23	1149	22	1380	40	75
RZ 17-2	A207	167956	882	160	0.34	b.d.	0.175	3.9	2.141	3.9	0.089	0.6	0.99	1041	38	1162	28	1396	12	75
RZ 17-2	A208	142613	785	167	1.15	0.2	0.175	2.7	2.148	2.8	0.089	0.8	0.96	1039	26	1165	20	1406	14	74
RZ 17-2	A225	136839	780	150	1.36	0.1	0.170	2.7	2.055	2.8	0.088	0.6	0.97	1010	25	1134	19	1378	12	73
RZ 17-2	A159	168196	1027	190	0.54	0.1	0.174	4.3	2.157	4.3	0.090	0.6	0.99	1032	41	1167	31	1429	12	72
RZ 17-2	A249	136643	675	117	0.60	0.1	0.167	2.5	2.042	2.6	0.089	0.6	0.97	994	23	1130	18	1400	12	71
RZ 17-2	A233	105362	463	91	1.76	2.3	0.156	4.4	1.833	5.8	0.085	3.8	0.76	934	39	1057	39	1321	74	71
RZ 17-2	A188	153525	766	143	0.99	b.d.	0.163	3.0	1.977	3.1	0.088	0.6	0.98	974	27	1108	21	1381	12	71
RZ 17-2	A131	142274	659	123	0.79	0.1	0.162	3.9	1.976	4.5	0.089	2.3	0.86	967	35	1107	31	1395	44	69
RZ 17-2	A182	145103	751	128	0.54	0.9	0.162	3.6	1.972	3.7	0.089	1.1	0.96	965	32	1106	25	1394	21	69
RZ 17-2	A184	131552	700	126	0.69	0.1	0.161	5.1	1.983	5.1	0.089	0.6	0.99	965	46	1110	35	1407	12	69
RZ 17-2	A181	182016	952	160	0.87	0.7	0.160	3.4	1.959	3.5	0.089	0.9	0.97	957	30	1102	24	1401	17	68
RZ 17-2	A135	160390	949	178	0.80	1.9	0.161	2.7	2.003	4.0	0.090	2.9	0.68	964	25	1116	27	1426	56	68
RZ 17-2	A248	133533	761	109	0.55	0.0	0.147	3.7	1.723	3.7	0.085	0.6	0.99	884	31	1017	24	1317	11	67
RZ 17-2	A244	122886	857	145	1.85	b.d.	0.157	2.5	1.925	2.6	0.089	0.6	0.97	938	22	1090	18	1408	11	67
RZ 17-2	A217	145475	932	206	1.55	1.5	0.159	6.5	1.975	6.9	0.090	2.5	0.93	951	57	1107	48	1428	47	67
RZ 17-2	A206	178965	914	150	1.04	0.1	0.155	2.7	1.906	2.7	0.089	0.6	0.97	930	23	1083	18	1406	12	66
RZ 17-2	A211	132844	751	151	1.37	b.d.	0.154	5.2	1.890	5.3	0.089	0.6	0.99	921	45	1078	36	1409	11	65
RZ 17-2	A250	179274	960	153	0.57	0.1	0.151	2.7	1.848	2.8	0.089	0.6	0.98	908	23	1063	19	1396	11	65
RZ 17-2	A235	131516	844	115	1.25	0.1	0.134	4.1	1.606	4.1	0.087	0.6	0.99	809	31	973	26	1363	12	59
RZ 17-2	A142	156911	916	141	0.48	0.7	0.139	2.6	1.713	2.8	0.089	1.0	0.93	838	20	1013	18	1414	19	59
RZ 17-2	A226	23935	345	44	0.26	b.d.	0.122	3.3	1.502	3.7	0.089	1.5	0.91	743	23	931	23	1408	29	53
RZ 17-2	A143	176952	1187	179	0.96	b.d.	0.116	6.3	1.396	6.4	0.087^d	1.1	0.99	707	43	887	39	1370	21	52
RZ 17-2	A139	175791	1276	151	0.99	b.d.	0.115	2.7	1.396	2.8	0.088	0.6	0.98	702	18	887	16	1383	11	51
RZ 17-2	A189	160347	947	133	0.93	0.1	0.115	3.9	1.399	3.9	0.088	0.7	0.99	702	26	888	23	1386	13	51
RZ 17-2	A158	142268	857	112	0.70	0.3	0.117	5.0	1.435	5.0	0.089	0.8	0.99	712	34	904	31	1407	15	51
RZ 17-2	A202	185627	1117	148	0.78	1.0	0.115	2.5	1.448	2.8	0.091	1.3	0.89	704	17	909	17	1448	24	49
RZ 17-2	A251	100161	818	99	0.41	0.3	0.112	4.7	1.376	4.8	0.089	0.8	0.98	684	31	879	29	1409	16	49
RZ 17-2	A219	126317	852	111	0.72	1.8	0.114	3.3	1.438	4.0	0.091	2.2	0.84	697	22	905	24	1453	41	48
RZ 17-2	A229	173497	1489	182	1.37	0.1	0.106	4.1	1.288	4.2	0.088	0.7	0.98	648	25	840	24	1389	14	47
RZ 17-2	A205	136853	776	98	0.70	1.5	0.106	2.7	1.302	3.2	0.089	1.6	0.86	649	17	846	18	1405	31	46
RZ 17-2	A213	216502	1473	155	1.00	0.0	0.104	2.8	1.270	2.9	0.089	0.5	0.98	637	17	832	16	1398	10	46
RZ 17-2	A167	154210	1431	135	0.90	0.1	0.086	4.9	1.044	5.0	0.088	0.6	0.99	531	25	726	26	1389	12	38
RZ 17-2	A156	139194	1644	146	1.00	0.5	0.082	3.3	1.007	3.3	0.090	0.8	0.97	505	16	707	17	1416	15	36
RZ 17-2	A174	164879	1206	112	1.18	0.2	0.081	6.9	1.008	6.9	0.090	0.6	1.00	505	34	708	36	1419	12	36
RZ 17-2	A165	137531	849	68	0.38	0.0	0.072	6.9	0.893	6.9	0.090	0.6	1.00	449	30	648	34	1423	11	32
RZ 17-2	A221	113098	780	64	0.68	0.3	0.056	9.8	0.690	9.9	0.089	0.8	1.00	351	34	533	42	1414	14	25
RZ 17-2	A254	76410	1046	69	1.47	0.0	0.051	3.8	0.621	3.9	0.088	0.8	0.98	323	12	491	15	1378	16	23
RZ 17-2	A141	152930	2154	121	0.84	0.2	0.040	10.4	0.487	10.4	0.088	0.7	1.00	253	26	403	35	1388	13	18
RZ 17-2	A132	250293	9698	412	3.26	0.0	0.037	9.5	0.445	9.7	0.087	1.6	0.99	234	22	373	31	1368	31	17
RZ 17-2	A161	99116	824	45	1.40	1.1	0.033	19.0	0.401	19.0	0.089	1.3	1.00	208	39	343	57	1402	25	15

[a] Within-run background-corrected mean ^{207}Pb signal. [b] U and Pb content and Th/U ratio were calculated relative to GJ-1 reference. [c] corrected for background and within-run Pb/U or Pb/Th fractionation and normalised to GJ-1 (ID-TIMS value/measured value); ^{207}Pb/^{235}U calculated using ^{207}Pb/^{206}Pb/(^{238}U/^{206}Pb × 1/137.88). [d] mass bias corrected by normalising to GJ-1 (ca. 0.5% per amu). [e] Error correlation defined as err^{206}Pb/^{238}U/err^{207}Pb/^{235}U. [f] degree of concordance=(^{238}U/^{206}Pb age×100/^{207}Pb/^{206}Pb age).
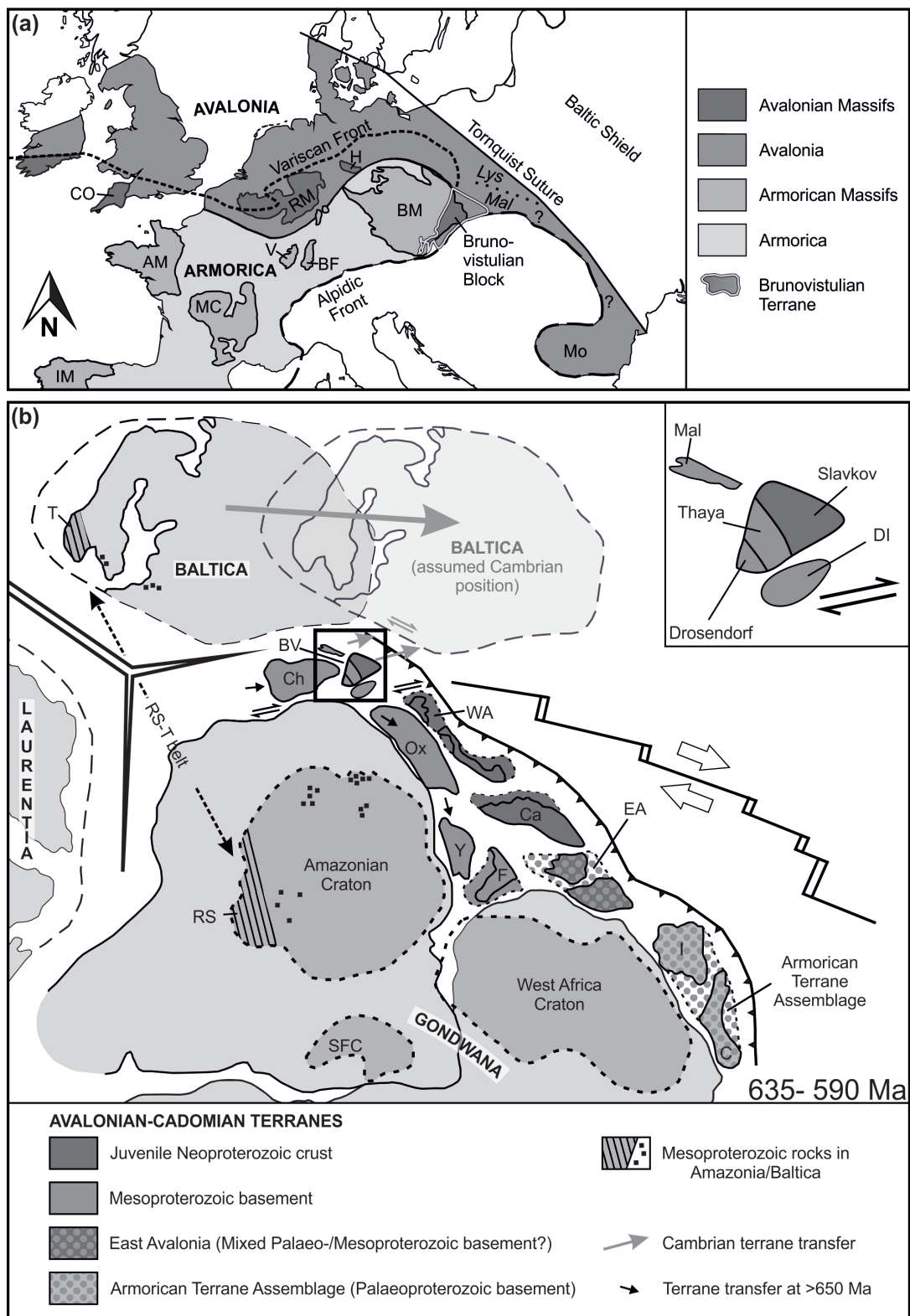
Figure 2: Palaeogeographic situation. (a) Terrane map of Central Europe according to (Stephan et al., 2019). The Drosendorf Unit is part of the Brunovistulian block. Both belonged to the Old Red Continent in the Devonian (as a part of the so-called Avalonian Europe). The Armorican superterrane (light grey) lay south of the main Variscan suture (i.e., south of the Rheic Ocean) before the Variscan orogeny (Linnemann et al., 2008; Kroner and Romer, 2013; Stephan et al., 2019). Modified after Lindner et al. (2020). (b) Palaeogeographic sketch showing the position of the Brunovistulian Plate in the Late Neoproterozoic. Modified after Nance et al. (2012), distribution of Mesoproterozoic rocks in Baltica and Amazonia from Johansson (2009). According to Lindner et al. (2020), the Drosendorf Unit was positioned close to Amazonia at that time. It was transferred from Amazonia to Baltice along with the Brunovistulian terrane in the Cambrian. Note that Armorica had a position close to Africa.

Abbreviations: AM: Armorican Massif; BF: Black Forest; BM: Bohemian Massif; BV: Brunovistulia; C: Cadomia; Ca: Carolina; Ch: Chortis Block; CO: Cornwall; DI: Dobrogea Istanbul terrane; EA: East Avalonia; F: Florida; H: Harz; IM: Iberian Massif; Lys: Lysogory; Mal: Małopolska; MC: Massif Central; Mo: Moesian Platform; Ox: Oaxaquia; RM: Rhenish Massif; RS: Rondonian–San Ignácio/Sunsás; SFC: São Francisco Craton; T: Telemarkia; V: Vosges; WA: West Avalonia; Y: Yucatan Block.

Figure 3: Polished surface and thin-section photographs of sample RZ 17-2. (a) Sample RZ 17-2 cut and polished. (b), (c) Rock structures in thin section under plane- (b) and cross-polarized (c) light. Readers are referred to the online version for the colour images.

4.3 Geochemistry

Two samples of the Hauergraben Gneiss were geochemically investigated (RZ 17-2 and RZ 17-2B). The results are shown in table 2. SiO_2 contents are 58.70 and 58.82 wt%, respectively. According to its normative modal composition (Mielke and Winkler, 1979; Janoušek et al., 2006), the rock can be described as quartzmonzonite (Streckeisen, 1974). In comparison to the Dobra Gneiss Type A and B data (Lindner et al., 2020), the Hauergraben Gneiss has lower SiO_2, higher Fe_2O_3 (5.96-6.11 wt%) and MgO (3.76-3.80 wt%). Furthermore, it has elevated Cr (103-116 ppm), Co (~18 ppm), Ni (~28 ppm), V(132-135 ppm) and Zn (53-56 ppm) contents (Fig. 7).

In the trace-element classification scheme of Pearce et al. (1984), the Hauergraben Gneiss classifies as volcanic arc granite, like both Dobra Gneiss types.

In a chondrite normalized REE element plot (Fig. 8a), the Hauergraben Gneiss sample shows a strong enrichment in the LREEs and a moderate enrichment of the HREEs. No appreciable Eu-anomaly is seen in this sample (Eu/Eu* = 0.97; calculated after Lawrence and Kamber, 2006). In an N-MORB normalized multi-elemental plot (Fig. 8b), peaks are observed for Ba, Sr, Nd and Gd, as well as elevated values for K, La, Ce and Pb. Negative spikes are present for Nb, Ta, Pb, P and Ti.

4.4 Mineral chemistry and geothermobarometry

4.4.1 Mineral compositions

Some representative mineral analyses are given in Table 3. The plagioclase crystals are widely homogenous with an An content of 27-38. K-feldspar has low albite contents (Ab11-14) and BaO contents between 1.31 and 1.47 wt%.
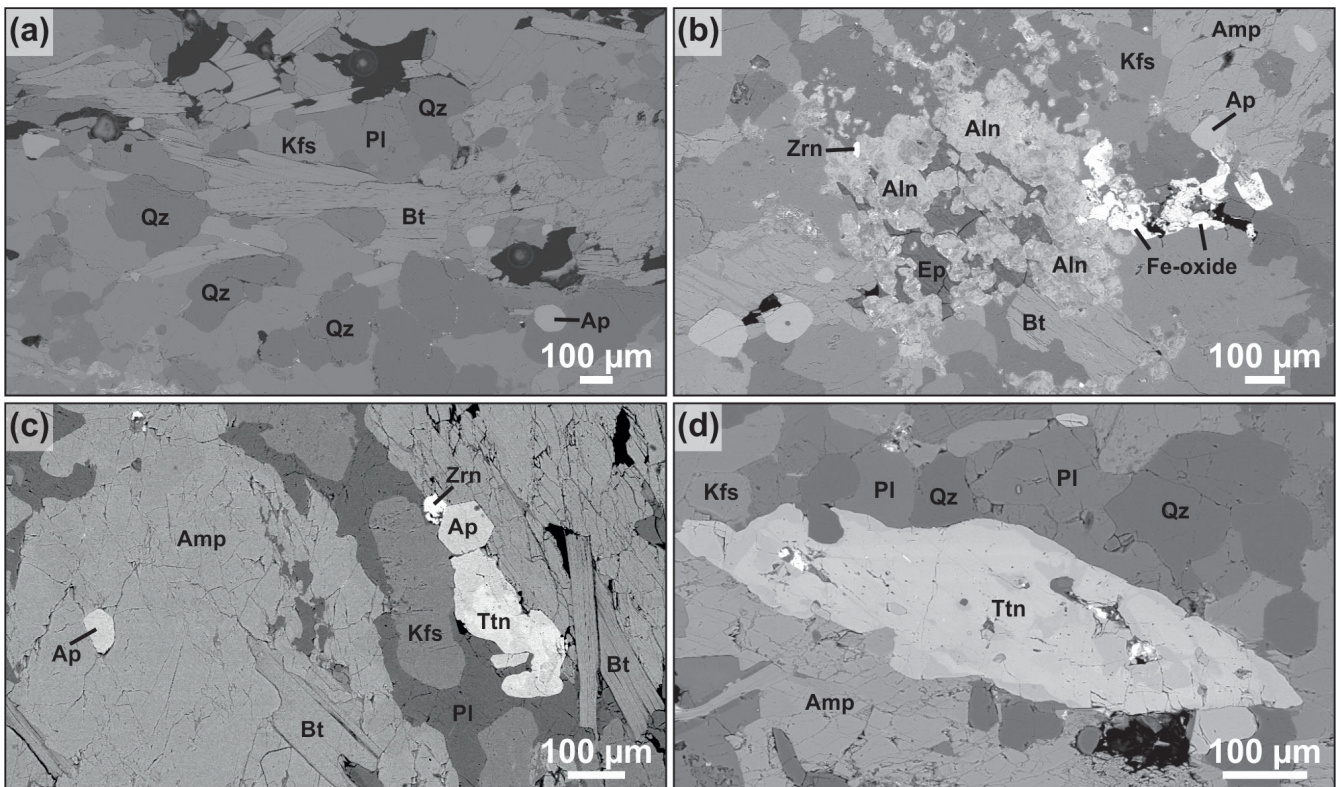
Figure 4: Back-scattered electron images of sample RZ 17-2. (a) Typical section of the sample, with K-feldspar, plagioclase, quartz, biotite and accessory apatite. (b) Patchy allanite and epidote surrounded by K-feldspar, amphibole and biotite, with accessory zircon and Fe-oxides. (c) A large amphibole crystal with K-feldspar, plagioclase and biotite, with additional accessory apatite, zircon and titanite. (d) A large titanite crystal surrounded by a matrix of K-feldspar, plagioclase, quartz and amphibole. Mineral abbreviations according to Whitney and Evans (2010).
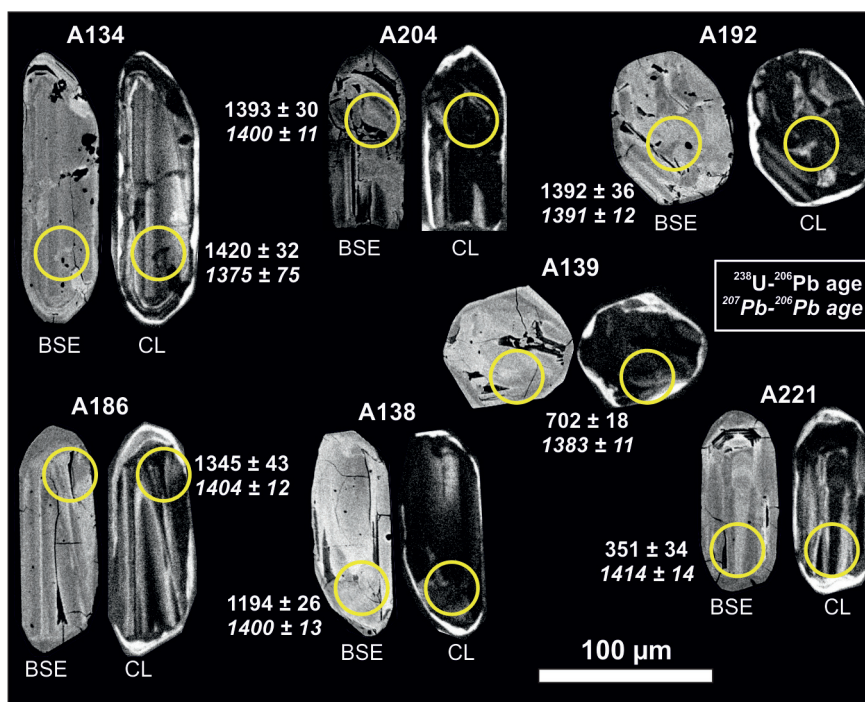
Figure 5: Back-scattered electron (BSE) and cathodoluminescence (CL) images of zircons from sample RZ 17-2. Circles indicate locations of LA-ICP-MS measuring spots (Ø 30μm). ^{238}U-^{206}Pb and ^{207}Pb-^{206}Pb (italics) ages are shown for each analysis. Errors are 2σ.

Amphibole is mainly edenite to pargasite (Fig. 9a; Leake et al., 1997). Small, patchy zones with darker BSE signal have the composition of magnesiohornblende (Fig. 9b) and occur near the margins of larger amphibole crystals, mostly in contact to feldspar (Fig. 10).

The K_2O ranges between 1.4 and 1.9 wt% in the edenites/pargasites, and between 0.5 and 1.2 wt% the magnesiohornblendes. The MgO/(MgO+FeO) ratio is between 0.38 and 0.43 in edenites/pargasites, and between 0.40 and 0.51 in the magnesiohornblendes. In the edenites/pargasites, F ranges between 0.59 and 0.89 wt%, and between 0.40 and 0.74 wt% in the magnesiohornblendes. Chlorine ranges between 0.03 and 0.08 wt% in pargasites/edenites, and between 0.02 and 0.10 wt% in the magnesiohornblendes.

Biotite generally has Mg/(Mg+Fe) ratios > 0.5 and Al^{IV} < 3, and, thus, represents phlogopite (Fig. 9c; Rieder et al., 1999). The Al^{IV} content (apfu) is generally very low (< 2.27), with one exception that has Al^{IV} of 2.74 (apfu). TiO_2 ranges between 1.24 and 2.83 wt%. Fluorine ranges between 1.22 and 1.47, chlorine between 0.10 and 0.17 wt%.

One analysed example of rare secondary chlorite had a Mg/(Mg+Fe) ratio of 0.52, and classifies as clinochlore (Bayliss, 1975).

4.4.2 Geothermobarometry

The mineral paragenesis amphibole plus plagioclase (+Kfs, Qz, Bt) is suitable for geothermobarometric calculations.

For the edenite/pargasite analyses, the empirical geothermobarometer of Zenk and Schulz (2004) gives an average temperature of 616±9 °C at an average pressure of 5.8±0.2 kbar. Temperatures obtained from the hornblende-plagioclase geothermometer of Holland and Blundy (1994) give 679±18 °C at an arbitrary pressure of 6 kbar. The empirical geothermometer of Otten (1984) gives an average temperature of 635±11 °C.

The magnesiohornblendes show an overall greater spread in composition, and, thus, also in the results of the geothermobarometric calculations. Calculated temperatures range between 482 and 570 °C at pressures between 3.0 and 4.7 kbar (Zenk and Schulz, 2004). Temperatures calculated from the Ti-in-hornblende thermometer (Otten, 1984) range between 586 and 646 °C for the magnesiohornblendes.

The Ti-in-biotite geothermometer of Henry et al. (2005) gives an average temperature of 600±12 °C, which is consistent with the geothermometric results for the edenite/pargasite analyses.

5. Discussion

5.1. The protolith of the Hauergraben Gneiss

The zircon population of the Hauergraben Gneiss gives unequivocal evidence that the rock is of igneous origin. We can infer this from the igneous zircon morphologies, from the dominantly magmatic zoning patterns, and, most importantly, from the fact that all zircons are of absolutely the same age (if we neglect the volumetrically minor metamorphic overgrowth rims). Our U-Pb data show that the magmatic formation of the Hauergraben Gneiss took place some 20 Ma before the Dobra Gneiss originated. Note, that the U-Pb ages of the Dobra
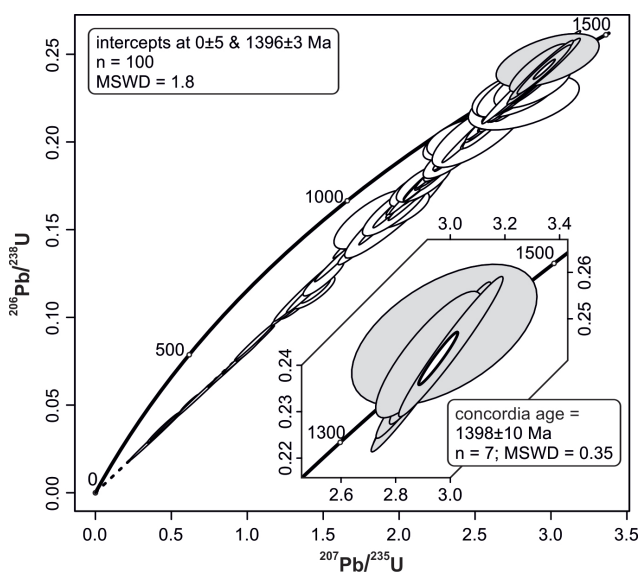
Figure 6: Concordia diagram for the dated Hauergraben Gneiss sample (RZ 17-2). Inset highlights the concordant analyses (grey ellipses) used for the calculation of the 1398±10 Ma concordia age.

and Hauergraben gneiss (1377±10 and 1398±10 Ma) are distinct within error and a cogenetic origin can therefore be ruled out. It is likely that the Hauergraben Gneiss represents a piece of a slightly older magmatic crust into which the protolith of the Dobra Gneiss intruded.

While the host Dobra Gneiss is a fairly normal granitic-granodioritic gneiss, the Hauergraben Gneiss exhibits an unusual mela-quartzmonzonitic composition, i.e., the rock has an extraordinary high K_2O and K-feldspar content considering its low SiO_2 and high maficity. This may eventually indicate metasomatic changes. On the other hand, such melagranitoids may form when lithospheric melts mix with crustal melts (Gerdes et al., 2000). A significant contribution of an enriched mantle source can also be inferred from the high contents of transitional metals (Ti, V, Cr, Mn, Fe, Co, Ni, Zn), which occur in combination with high LREE abundances. Many of these elements are regarded as immobile and their contents therefore likely represent a primary magmatic signature.

Overall, the trace and REE patterns of the Hauergraben Gneiss are interpretable in terms of subduction related magmatism (enrichment of LILE and LREEs, pronounced negative Nb, Ta and Ti anomalies in normalized multi-elemental plots - Fig. 8). We interpret that the gneiss represents an early evolution stage of the Mesoproterozoic Drosendorf arc, which is mainly represented by the 1.38 Ga old Dobra Gneiss Type A.

### 5.2 Metamorphic history of the Hauergraben Gneiss
We suppose that the magmatic protolith of the Hauergraben Gneiss experienced a first metamorphic overprint at the latest during the Cadomian orogeny, like the host Dobra Gneiss Type A, as evidenced by zircon rim ages (Gebauer and Friedl, 1994). Cadomian metamorphism may have occurred in the contact aureole of the ~580 Ma

Table 2: Whole-rock major-(wt%) and trace-element (ppm) composition of the Hauergraben Gneiss samples RZ 17-2 and RZ 17-2B.

	Sample	RZ 17-2	RZ 17-2B
	Coordinates N	48.577	48.577
	E	15.423	15.423
X-ray fluorescence (University of Salzburg, Austria)	SiO_2	58.70	58.82
	TiO_2	0.59	0.58
	Al_2O_3	14.31	14.43
	Fe_2O_3	6.11	5.96
	MnO	0.09	0.09
	MgO	3.76	3.80
	CaO	5.81	5.90
	Na_2O	2.44	2.39
	K_2O	4.89	4.70
	P_2O_5	0.81	0.83
	SO_3	0.01	0.02
	F	0.33	0.31
	LOI	1.40	1.36
	Sum	99.25	99.19
	Rb	120	118
	Sr	2334	2318
	Ba	3692	3557
	Th	29	34
	La	158	175
	Ce	378	369
	Nd	135	141
	Ga	14	15
	Nb	23	23
	Zr	268	252
	Y	25	22
	Sc	20	18
	Pb	4	4
	Zn	55	53
	V	135	132
	Co	18	18
	Cr	103	116
	Ni	28	28
ICP-MS (ALS Laboratories, Laughrea, Ireland)	La	155.5	
	Ce	345.0	
	Pr	30.8	
	Nd	123.5	
	Sm	14.45	
	Eu	3.57	
	Gd	9.58	
	Tb	1.09	
	Dy	5.24	
	Ho	1.02	
	Er	2.35	
	Tm	0.29	
	Yb	2.00	
	Lu	0.30	
	Hf	7.3	
	U	5.23	
	Cs	1.62	
	Ta	1.2	
	Eu/Eu*	0.97	

LOI = loss on ignition

$Eu/Eu^* = Eu_N / (Sm_N^2 * Tb_N)^{(1/3)}$
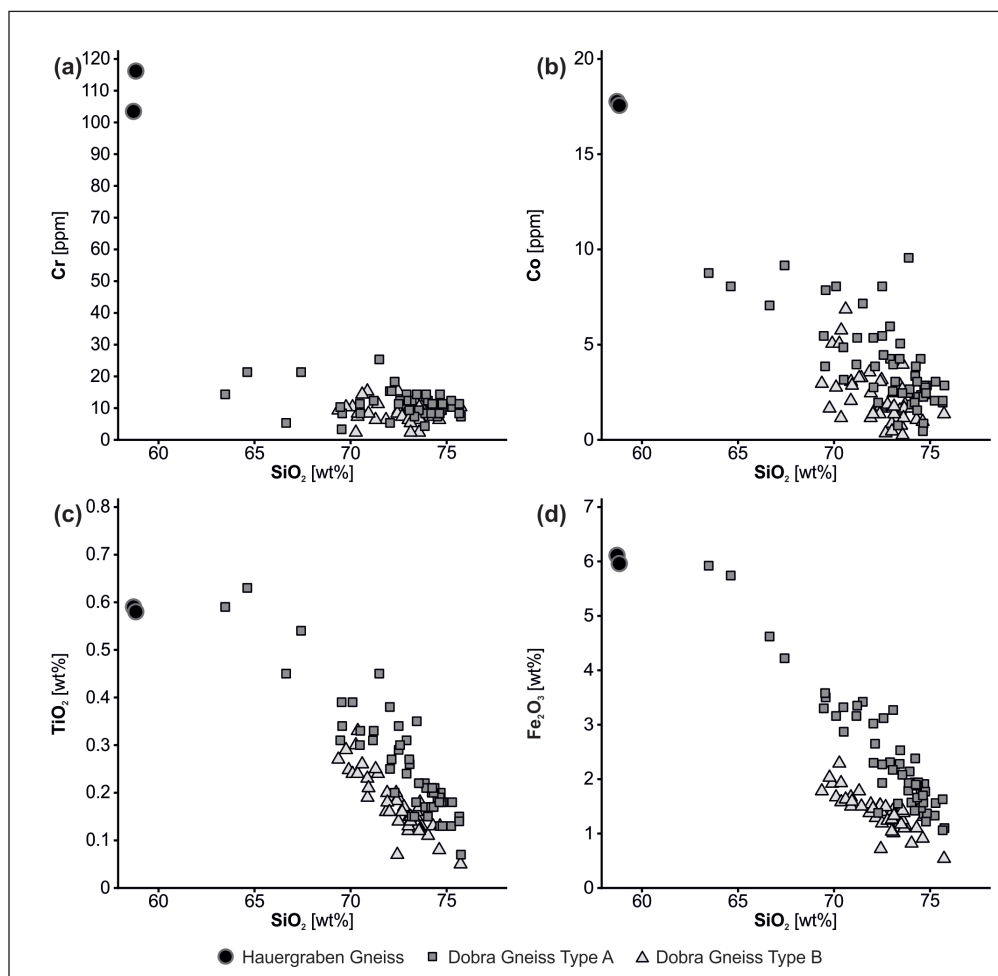
Figure 7: Geochemical diagrams with Hauergraben Gneiss and Dobra Gneiss Type A and B data (Lindner et al., 2020). (a) SiO_2 vs Cr; (b) SiO_2 vs Co; (c) SiO_2 vs TiO_2; (d) SiO_2 vs Fe_2O_3.

old Dobra Gneiss Type B (Lindner et al., 2020) or during an earlier Cadomian regional metamorphic event (Sorger et al., 2020). However, with the potential exception of small metamorphic zircon overgrowths, no mineral relics from this time survived.

Sorger et al. (2020) have shown that parts of the Drosendorf Unit received an early Variscan metamorphic overprint at ~370 Ma. We see no evidence for this event in the Hauergraben Gneiss, however, its traces may have been completely obliterated during the main Variscan (Visean) regional metamorphism. According to amphibole thermobarometry, the latter metamorphic event has reached peak *PT* conditions of ~620 °C and 6 kbar in the Hauergraben Gneiss. This fits broadly to published peak *PT* data for the Dobra Gneiss (Büttner and Kruhl, 1997) and rocks from the middle sector of the Drosendorf Unit in the Kamp valley (Sorger et al., 2020).

Partial recrystallization of the edenitic/pargasitic primary amphibole to secondary magnesiohornblende likely represents the retrograde metamorphic path of the Drosendorf Unit. Interestingly, in other parts of the Drosendorf Unit (i.e. further East near Spitz), such a retrograde metamorphic event is not recorded in amphiboles (Lindner and Finger, 2018).

5.3 The Drosendorf Unit: A prospective hunting ground for pre-Cadomian rocks

Although pre-Cadomian zircons are commonly found as detritus in Palaeozoic and younger sediments (Neubauer et al., 2001; Siegesmund et al., 2007; Košler et al., 2013), remnants of pre-Cadomian rocks are an absolute rarity in Austria and beyond in the entire Variscides. The proof of an 1.38 Ga protolith age for the Dobra Gneiss in the 1990's (Gebauer and Friedl, 1994) was thus a bit of a sensation. However, already a few years earlier, Frank et al. (1990) proposed that the metasedimentary rocks of the Drosendorf Unit could be of Tonian age, based on results of a Sr isotope investigation.

The idea that large parts of the Drosendorf Unit could be pre-Cadomian has received much support in the recent past. For instance, Gerdes and Finger (2005) dated detrital zircons in a quartzite from the Drosendorf Unit and found that these were all extremely old (>1.5 Ga). They discovered the oldest zircons from Austria (3.4 Ga) in this rock. A metarhyolite with a zircon age of ~1.25 Ga was found near Raabs by Mayer et al. (2013) and, according to the map of Waldmann (1951), this rock may also be a part of the Drosendorf Unit. Furthermore, 2 Ga old zircons from an amphibolite of the Gföhl Unit (Raabs Unit
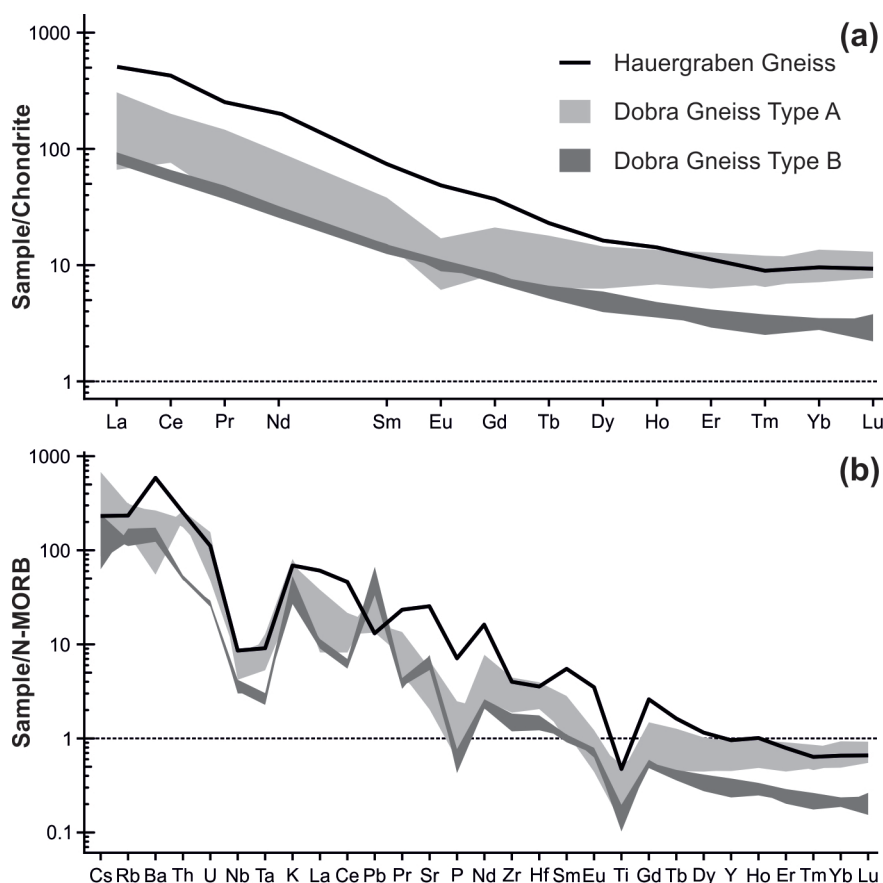
Figure 8: Normalized multi-elemental plots for the Hauergraben Gneiss in comparison to Dobra Gneiss Type A and B (Lindner et al., 2020). (a) Chondrite normalized (Boynton, 1984) REE plot. (b) N-MORB normalized (Sun and McDonough, 1989) multi-elemental plot.

of Thiele, 1984) were reported by Mayer et al. (2013), but it is not clear whether these Early Proterozoic zircons are inherited or autocrystic (in which case they would date the age of the basaltic protolith). Sorger et al. (2020) and Lindner et al. (2020) recently presented LA-ICP-MS U-Pb age data for detrital zircons from metapelitic paragneiss samples of the Drosendorf Unit, which imply that the sedimentary protoliths of these rocks were deposited in the early Neoproterozoic like the calcareous protoliths of the Drosendorf marbles (Frank et al., 1990).

According to Lindner et al. (2020), the Drosendorf Unit was positioned close to the Amazonian craton until the early Cambrian. At that time, the Drosendorf Unit left Gondwana/Amazonia as a part of the Brunovistulian Terrane (Fig. 2b). Most published work is focused on the tectonic position of the Drosendorf Unit in the Variscan orogen. However, the earlier Amazonian history of the Drosendorf Unit involves a very long evolution, at least from 1.4 to 0.6 Ga, which is barely constrained and little understood: At the end of the Precambrian, the Drosendorf Unit was part of the Andean-type Avalonian-Cadomian Orogen, which extended at that time along the north Gondwana coast (Fig. 2b). The Avalonian-Cadomian Orogeny has left the following traces in the Drosendorf Unit: 1) Formation of the granodioritic Spitz Gneiss at 614 Ma (Friedl et al., 2004; Lindner and Finger, 2018); 2) Formation of the Dobra Gneiss Type B, a 580-570 Ma granitoid pluton, which represents a second pulse of Late Neoproterozoic

volcanic arc magmatism; 3) Late Neoproterozoic metamorphism in Dobra Gneiss Type A in the form of metamorphic zircon rims with an age of ~600 Ma (Gebauer and Friedl, 1994); and 4) Monazite relics, dated at ~650 Ma, in paragneiss of the Drosendorf Unit (Sorger et al., 2020).

Notably, most of the sedimentary rocks of the Drosendorf Unit were probably deposited several hundred million years earlier, i.e. during the Early Neoproterozoic (Frank et al., 1990; Lindner et al., 2020; Sorger et al., 2020). These sediments may have originated in basins that opened in the forefield of the Amazonian craton during the suturing of the Rodinia supercontinent. They were probably accreted to the Avalonian-Cadomian Orogen later on. It is well possible that the Hauergraben Gneiss, Dobra Gneiss Type A and the metasediments of the Drosendorf Unit are completely unrelated and that they were located far apart from each other in the early Neoproterozoic. Indeed, Lindner et al. (2020) found that ~1.4 Ga detrital zircons are surprisingly rare in the paragneiss occurrences east of the Dobra Gneiss, which means that the protolithic clastic sediments were not sourced from the Hauergraben or Dobra Gneiss Type A protolith (or age-equivalent magmatic rocks). Interestingly, they were sourced from a magmatic province with a 1.0-1.3 Ga age.

Prior to the Rodinia break-up, in the Mesoproterozoic period, the Hauergraben Gneiss and the Dobra Gneiss Type A were likely part of the Rondonian-Telemarkian
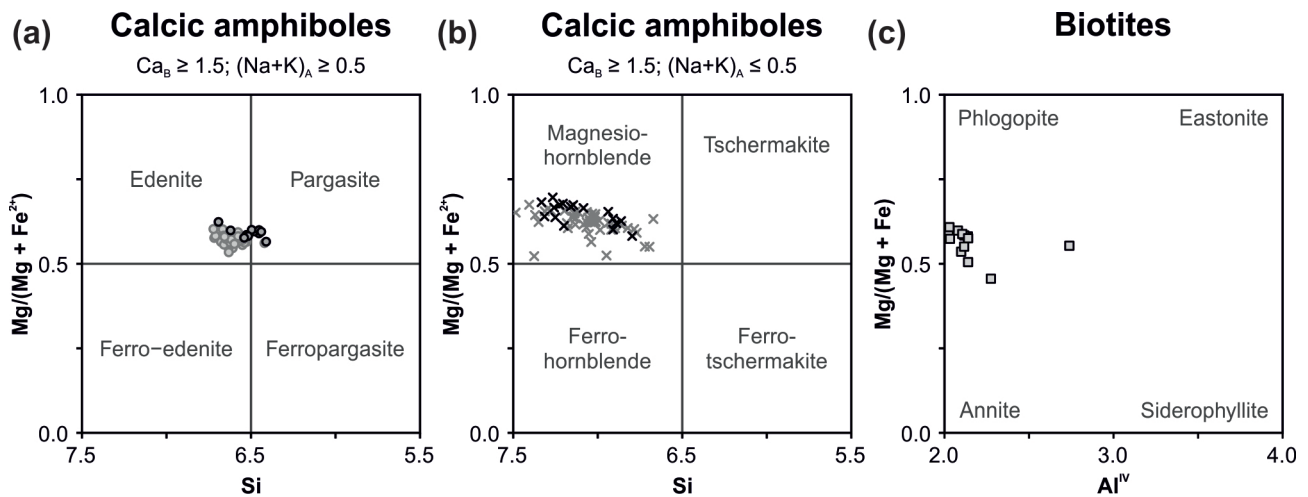
Figure 9: Mineral chemistry classification diagrams (apfu). (a), (b) Amphibole classification diagram for calcic amphiboles after Leake et al. (1997). Fe^{2+} calculated after Holland and Blundy (1994) from FeO_{tot}. Black symbols: EPMA analyses; Grey symbols: SEM analyses. (c) Biotite classification diagram after Rieder et al. (1999). Total iron calculated as Fe^{2+}.

orogenic belt, which involved a series of accreted Meso-proterozoic volcanic arcs at the western side of the Columbia supercontinent (Johansson 2009, 2014; and references therein). Rocks with compositions and ages similar those rocks are known for instance in Bolivia (Matos et al., 2009, 2017) and also from southern Sweden (Åhäll et al., 1997).

What are the chances to find rocks with a formation age greater than 1.4 Ga in the Drosendorf Unit in future studies? We think that they are good, because such rocks could locally be preserved within or around the Dobra Gneiss Type A. Notably, isotope data (Liew and Hofmann, 1988) indicate that the Mesoproterozoic Dobra Gneiss arc system was built within much older continental crust. Furthermore, we know from detrital zircon age spectra in the paragneiss and quartzite samples that a reworking

of Palaeoproterozoic and even Archean crust has taken place here and it is not impossible that larger fragments of such older cratonic crust are somewhere intercalated in these rocks.

6. Conclusions

- The Hauergraben Gneiss is, according to the present state of knowledge, the oldest rock in Austria with a magmatic formation age of 1.40 Ga. It forms small mafic inlayers in the 1.38 Ga old Dobra Gneiss Type A of the Drosendorf Unit.
- The Hauergraben Gneiss has a mela-quartzmon-zonitic composition. It differs from the host Dobra Gneiss by higher transitional metal contents (Ti, V, Cr, Mn, Fe, Co, Ni, Zn), as well as higher MgO, Ba, Sr and LREE contents. These geochemical features
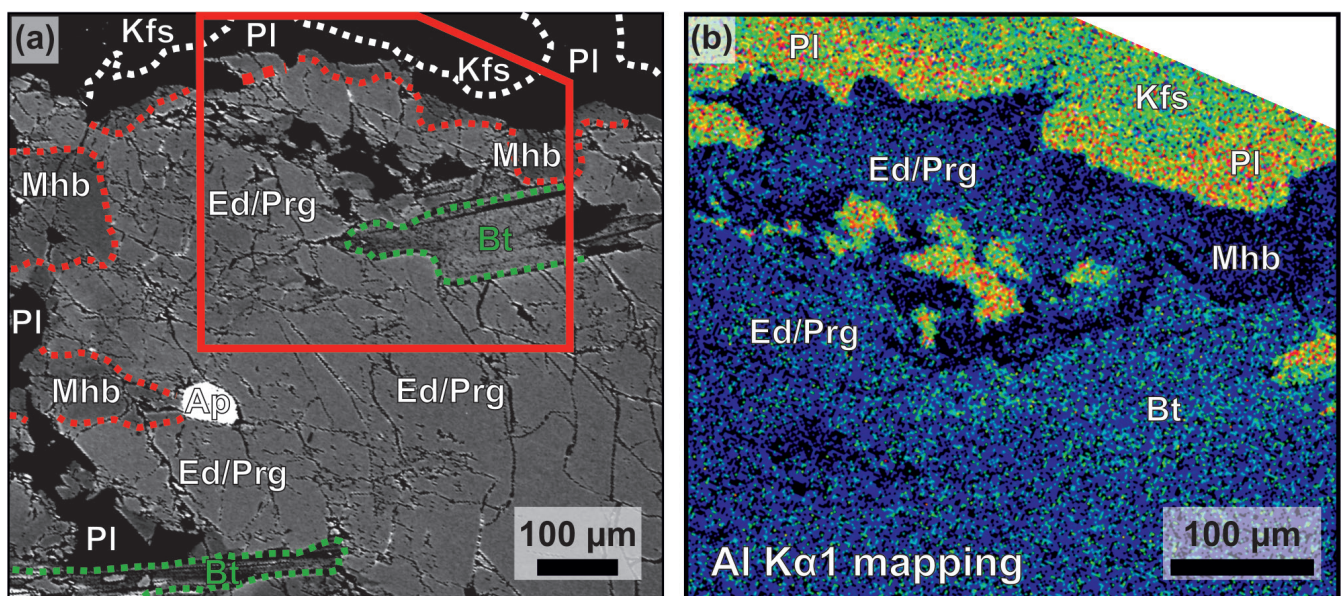
Figure 10: Back-scattered electron image and Al Kα1 x-ray map showing the partial replacement of edenite/pargasite through magnesiohornblende. (a) BSE image. (b) Elemental mapping (Al Kα1). Readers are referred to the online version for the colour image.

Table 3: Representative mineral analyses from the Hauergraben Gneiss sample RZ 17-2.

Mineral	Prg	Prg	Ed	Ed	Mhb1	Mhb1	Mhb1	Mhb2	Mhb2	Mhb2		Bt	Bt	Bt		Pl	Pl	Pl	Kfs	Kfs	Kfs
SiO_2	43.11	42.96	43.31	43.23	45.82	46.23	46.37	48.38	49.12	47.92		37.87	37.73	38.40		61.44	60.31	59.77	63.97	63.78	64.44
TiO_2	0.79	0.58	0.64	0.48	0.52	0.53	0.56	0.53	0.31	0.64		1.71	1.66	1.57		n.a.	n.a.	n.a.	n.a.	n.a.	n.a.
Al_2O_3	11.55	12.03	11.29	11.56	8.53	8.33	8.13	6.94	5.10	6.44		14.21	14.66	14.12		24.34	23.05	24.95	18.72	18.76	18.13
Cr_2O_3	0.48	0.63	0.22	0.01	0.03	0.13	0.55	0.40	0.18	0.03		0.67	0.68	0.36		b.d.l.	0.25	b.d.l.	b.d.l.	b.d.l.	0.07
FeO_{tot}	16.10	15.64	15.82	15.51	15.41	14.77	15.69	14.51	15.18	14.79		17.05	17.91	18.64		0.07	0.27	0.25	0.05	0.04	b.d.l.
MnO	0.27	0.31	0.28	0.27	0.29	0.26	0.29	0.26	0.27	0.32		0.16	0.19	0.21		n.a.	n.a.	n.a.	n.a.	n.a.	n.a.
MgO	10.55	10.47	10.46	10.72	11.15	11.94	11.84	13.01	12.66	11.76		13.23	13.19	13.09		n.a.	n.a.	n.a.	n.a.	n.a.	n.a.
Na_2O	1.34	1.42	1.30	1.33	0.90	1.09	1.20	0.98	0.74	0.90		0.14	0.08	0.09		7.08	7.07	6.82	1.37	1.36	1.29
K_2O	1.72	1.86	1.72	1.70	1.07	1.09	1.10	0.91	0.52	0.74		9.42	9.74	9.66		0.35	0.22	0.29	14.41	14.59	14.56
CaO	11.85	11.38	11.72	11.85	11.95	11.90	11.93	11.96	12.03	11.93		0.18	0.12	0.15		6.39	6.23	6.64	0.07	0.07	0.07
BaO	b.d.l.	b.d.l.	b.d.l.	b.d.l.	b.d.l.	0.01	b.d.l.	b.d.l.	b.d.l.	b.d.l.		0.24	0.25	0.08		0.02	0.01	b.d.l.	1.46	1.36	1.38
F	0.67	0.69	0.00	0.59	0.59	0.63	0.58	0.60	0.64	0.40		1.22	1.44	1.47		n.a.	n.a.	n.a.	n.a.	n.a.	n.a.
Cl	0.07	0.03	0.06	0.05	0.10	0.04	0.03	0.01	0.04	0.05		0.17	0.10	0.16		n.a.	n.a.	n.a.	n.a.	n.a.	n.a.
Total	98.50	97.97	97.51	97.31	96.34	96.95	98.26	98.49	96.80	95.92		96.26	97.76	98.00		99.71	97.40	98.76	100.10	100.05	100.00
Number of ions on the basis of:																					
	23 O	23 O	23 O	23 O	23 O	23 O	23 O	23 O	23 O	23 O		22 O	22 O	22 O		8 O	8 O	8 O	8 O	8 O	8 O
Si	6.46	6.46	6.53	6.50	6.91	6.91	6.89	7.09	7.32	7.20	Si	5.76	5.69	5.78	Si	2.73	2.75	2.69	2.97	2.96	2.99
Al^{IV}	1.54	1.54	1.47	1.50	1.09	1.09	1.11	0.91	0.68	0.80	Al^{IV}	2.24	2.31	2.22	Al	1.28	1.24	1.32	1.02	1.03	0.99
Sum	8.00	8.00	8.00	8.00	8.00	8.00	8.00	8.00	8.00	8.00	Sum	8.00	8.00	8.00	Sum	4.01	3.99	4.01	3.99	3.99	3.99
Al^{VI}	0.50	0.59	0.54	0.55	0.43	0.38	0.32	0.28	0.21	0.34	Al^{VI}	0.31	0.29	0.28	Ca	0.30	0.30	0.32	0.00	0.00	0.00
Ti	0.09	0.07	0.07	0.05	0.06	0.06	0.06	0.06	0.03	0.07	Ti	0.20	0.19	0.18	Na	0.61	0.62	0.60	0.12	0.12	0.12
$Fe^{3+}*$	0.36	0.37	0.31	0.33	0.26	0.29	0.32	0.32	0.29	0.17					K	0.02	0.01	0.02	0.85	0.87	0.86
Mg	2.35	2.35	2.35	2.40	2.51	2.66	2.62	2.84	2.81	2.63	Mg	3.00	2.96	2.94	Ba	0.00	0.00	0.00	0.03	0.02	0.03
Mn	0.03	0.04	0.04	0.03	0.04	0.03	0.04	0.03	0.03	0.04	Mn	0.02	0.02	0.03	Sum	0.93	0.94	0.93	1.01	1.02	1.01
$Fe^{2+}*$	1.66	1.59	1.68	1.62	1.68	1.56	1.63	1.45	1.60	1.69	Fe	2.17	2.26	2.35	mol. %						
Ca_C	0.01	0.00	0.01	0.01	0.03	0.02	0.01	0.01	0.02	0.05					An	0.33	0.32	0.34	0.00	0.00	0.00
C	5.00	5.00	5.00	5.00	5.00	5.00	5.00	5.00	5.00	5.00	Sum	5.69	5.73	5.76	Ab	0.65	0.66	0.64	0.13	0.12	0.12
Ca_B	1.89	1.83	1.88	1.90	1.91	1.89	1.89	1.87	1.90	1.87	Ca	0.03	0.02	0.02	Or	0.02	0.01	0.02	0.87	0.87	0.88
Na_B	0.11	0.16	0.12	0.10	0.09	0.11	0.11	0.13	0.10	0.13	Na	0.04	0.02	0.03							
Fe_B	0.00	0.01	0.00	0.00	0.00	0.00	0.00	0.00	0.00	0.00	K	1.83	1.87	1.85							
B	2.00	2.00	2.00	2.00	2.00	2.00	2.00	2.00	2.00	2.00	Sum										
Na_A	0.28	0.25	0.26	0.29	0.17	0.20	0.24	0.15	0.12	0.13	F	0.59	0.69	0.70							
K_A	0.33	0.36	0.33	0.33	0.21	0.21	0.21	0.17	0.10	0.14	Cl	0.04	0.03	0.04							
A	0.61	0.61	0.59	0.61	0.38	0.41	0.45	0.32	0.22	0.27											
1-A	0.39	0.39	0.41	0.39	0.62	0.59	0.55	0.68	0.78	0.73											

*Fe^{2+} and Fe^{3+} calculated from FeO_{tot} after Holland and Blundy (1994)
Mineral abbreviations according to Whitney and Evans (2010). n.a. - not analysed; b.d.l. - below the limit of detection

imply an input from a lithospheric mantle source. The slight but significant age difference indicates that the Hauergraben Gneiss is not fully cogenetic with the Dobra Gneiss Type A.

- Both the Dobra Gneiss and the Hauergraben Gneiss likely formed in a Mesoproterozoic volcanic arc setting in the Rondonian–San Ignácio/Sunsás orogen of the Amazonian Craton.
- Amphibole thermobarometry indicates that the Hauergraben Gneiss experienced *P-T* conditions of ~600 °C and 6 kbar during the Variscan orogeny. The peak metamorphic amphibole (edenite/pargasite) is partly replaced by secondary magnesiohornbelnde.

References
Åhäll, K., Samuelsson, L., Persson, P., 1997. Geochronology and structural setting of the 1.38 Ga Torpa granite; implications for charnockite formation in SW Sweden. *GFF*, 119, 37–43, https://doi.org/10.1080/11035899709546451.

Bayliss, P., 1975. Nomenclature of the Trioctahedral Chlorites. *Canadian Mineralogist*, 13, 178–180.

Boynton, W. V., 1984. Cosmochemistry of the rare earth elements: meteorite studies. *In*: Henderson, P. (ed.) *Rare Earth Element Geochemistry*. Elsevier B.V., 63–114., https://doi.org/10.1016/B978-0-444-42148-7.50008-3.

Büttner, S., Kruhl, J.H., 1997. The evolution of a late-Variscan high-T/low-P region: the southeastern margin of the Bohemian massif. *Geologische Rundschau*, 86, 21–38, https://doi.org/10.1007/s005310050119.

Cooke, R.A., O'Brien, P.J., Carswell, D.A., 2000. Garnet zoning and the identification of equilibrium mineral compositions in high-pressure-temperature granulites from the Moldanubian Zone, Austria. *Journal of Metamorphic Geology*, 18, 551–569, https://doi.org/10.1046/j.1525-1314.2000.00273.x.

Dallmeyer, R.D., Neubauer, F., Höck, V., 1992. Chronology of late Paleozoic tectonothermal activity in the southeastern Bohemian Massif, Austria (Moldanubian and Moravo-Silesian zones): 40Ar/39Ar mineral age controls. *Tectonophysics*, 210, 135–153, https://doi.org/10.1016/0040-1951(92)90132-P.

Dudek, A., 1980. The crystalline basement block of the outer Carpathians in Moravia. *Rozpravy Československe Akademie věd*, 90, 1–85.

Faryad, S.W., Racek, M., Lexa, O., 2011. Eclogite , Garnet Peridotite , Garnet Pyroxenite and HP Granulite in the Gföhl Unit. *GeoLines*, 23, 106–111.

Finger, F., Schubert, G., 2015. Die Böhmische Masse in Österreich : Was gibt es Neues? *Abhandlungen der Geologischen Bundesanstalt*, 64, 167–179.

Finger, F., Steyrer, H.P., 1995. A Tectonic Model for the Eastern Variscides - Indications from a Chemical Study of Amphibolites in the South-Eastern Bohemian Massif. *Geologica Carpathica*, 46, 137–150.

Finger, F., Frasl, G., Höck, V., Steyrer, H.P., 1989. The granitoids of the Moravian Zone of northeast Austria: Products of a Cadomian active continental margin? *Precambrian Research*, 45, 235–245, https://doi.org/10.1016/0301-9268(89)90042-9.

Finger, F., Hanžl, P., Pin, C., von Quadt, A., 2000. The Brunovistulian: Avalonian Precambrian at the eastern end of the Central European variscides? *Geological Society, London, Special Publications*, 179, 103–112, https://doi.org/10.1144/GSL.SP.2000.179.01.08.

Frank, W., Hammer, S., Popp, F., Scharbert, S., Thöni, M., 1990. Isotopengeologische Neuergebnisse zur Entwicklungsgeschichte der Böhmischen Masse: Proterozoische Gesteinsserien und Variszische Hauptorogenese. *Österr. Beitr. Met. Geoph.*, H3, 185–228.

Frasl, G., 1970. Zur Metamorphose und Abgrenzung der Moravischen Zone im niederösterreichischen Waldviertel. *Nachrichten der Deutschen Geologischen Gesellschaft*, 2, 55–61.

Friedl, G., 1997. *U/Pb -Datierungen an Zirkonen Und Monaziten Aus Gesteinen Vom Österreichischen Anteil Der Böhmischen Masse*.

Friedl, G., Finger, F., McNaughton, N.J., Fletcher, I.R., 2000. Deducing the ancestry of terranes: SHRIMP evidence for South America-derived Gondwana fragments in central Europe. *Geology*, 28, 1035–1038, https://doi.org/10.1130/0091-7613(2000)28<1035:DTAOTS>2.0.CO;2.

Friedl, G., Finger, F., Paquette, J.L., von Quadt, A., McNaughton, N.J., Fletcher, I.R., 2004. Pre-Variscan geological events in the Austrian part of the Bohemian Massif deduced from U-Pb zircon ages. *International Journal of Earth Sciences*, 93, 802–823, https://doi.org/10.1007/s00531-004-0420-9.

Fritz, H., Neubauer, F., 1993. Kinematics of crustal stacking and dispersion in the south-eastern Bohemian Massif. *Geologische Rundschau*, 82, 556–565, https://doi.org/10.1007/BF00212416.

Fuchs, G., 1970. Bericht 1969 über geologische Aufnahmen auf den Blättern Gföhl (20) und Horn (21). *Verh Geol Bundesanst*, A26–A27.

Fuchs, G., 1971. Zur Tektonik des östlichen Waldviertels (N.Ö.). *Verhandlungen der Geologischen Bundesanstalt*, 1971, 424–440.

Fuchs, G., 1976. Zur Entwicklung der Böhmischen Masse. *Jahrbuch der Geologischen Bundesanstalt*, 119, 45–61.

Fuchs, G., Matura, A., 1976. Zur Geologie des Kristallins der südlichen Böhmischen Masse. *Jahrbuch der Geologischen Bundesanstalt*, 119, 1–43.

Gebauer, D., Friedl, G., 1994. A 1.38 Ga protolith age for the Dobra orthogneiss (Moldanubian Zone of the southern Bohemian Massif, NE-Austria): Evidence from ion-microprobe (SHRIMP) dating of zircon. *Journal of the Czech Geological Society*, 39, 34–35.

Gerdes, A., Finger, F., 2005. Über die ältesten Zirkone Österreichs und neue Möglichkeiten in der Grundgebirgsforschung durch Einsatz moderner Laser-Ablation-ICP-MS Zirkonanalytik. *Mitteilungen der Österreichischen Mineralogischen Gesellschaft*, 151, 44.

Gerdes, A., Worner, G., Finger, F., 2000. Hybrids, magma mixing and enriched mantle melts in post-collisional Variscan granitoids: the Rastenberg Pluton, Austria. *Geological Society London, Special Publications*, 179, 415–431, https://doi.org/10.1144/GSL.SP.2000.179.01.25.

Gerdes, A., Friedl, G., Parrish, R.R., Finger, F., 2003. High-resolution geochronology of Variscan granite emplacement the South Bohemian Batholith. *Journal of the Czech Geological Society*, 48, 53–54.

Henry, D.J., Guidotti, C. V., Thomson, J.A., 2005. The Ti-saturation surface for low-to-medium pressure metapelitic biotites: Implications for geothermometry and Ti-substitution mechanisms. *American Mineralogist*, 90, 316–328, https://doi.org/10.2138/am.2005.1498.

Holland, T.J.B., Blundy, J., 1994. Non-ideal interactions in calcic amphiboles and their bearing on amphibole-plagioclase thermometry. *Contributions to Mineralogy and Petrology*, 116, 433–447, https://doi.org/10.1007/BF00310910.

Janoušek, V., Farrow, C.M., Erban, V., 2006. Interpretation of whole-rock geochemical data in igneous geochemistry: Introducing Geochemical Data Toolkit (GCDkit). *Journal of Petrology*, 47, 1255–1259, https://doi.org/10.1093/petrology/egl013.

Johansson, Å., 2009. Baltica, Amazonia and the SAMBA connection-1000 million years of neighbourhood during the Proterozoic? *Precambrian Research*, 175, 221–234, https://doi.org/10.1016/j.precamres.2009.09.011.

Johansson, Å., 2014. From Rodinia to Gondwana with the 'SAMBA' model-A distant view from Baltica towards

Amazonia and beyond. *Precambrian Research*, 244, 226–235, https://doi.org/10.1016/j.precamres.2013.10.012.

Klötzli, U.S., Parrish, R.R., 1996. Zircon U/Pb and Pb/Pb geochronology of the Rastenberg granodiorite, South Bohemian Massif, Austria. *Mineralogy and Petrology*, 58, 197–214, https://doi.org/10.1007/BF01172096.

Košler, J., Konopásek, J., Sláma, J., Vrána, S., 2013. U–Pb zircon provenance of Moldanubian metasediments in the Bohemian Massif. *Journal of the Geological Society*, 171, 83–95, https://doi.org/10.1144/jgs2013-059.

Kossmat, F., 1927. Gliederung des varistischen Gebirgsbaues. *Abhandlungen des Sächsischen Geologischen Landesamtes*, 1, 1–39.

Kroner, U., Romer, R.L., 2013. Two plates - Many subduction zones: The Variscan orogeny reconsidered. *Gondwana Research*, 24, 298–329, https://doi.org/10.1016/j.gr.2013.03.001.

Lawrence, M.G., Kamber, B.S., 2006. The behaviour of the rare earth elements during estuarine mixing-revisited. *Marine Chemistry*, 100, 147–161, https://doi.org/10.1016/j.marchem.2005.11.007.

Leake, B.E., Woolley, A.R., et al., 1997. Nomenclature of Amphiboles: Report of the Subcommittee on Amphiboles of the International Mineralogical Association Commission on New Minerals and Mineral Names. *Mineralogical Magazine*, 61, 295–321, https://doi.org/10.1180/minmag.1997.061.405.13.

Liew, T.C., Hofmann, A.W., 1988. Precambrian crustal components, plutonic associations, plate environment of the Hercynian Fold Belt of central Europe: Indications from a Nd and Sr isotopic study. *Contributions to Mineralogy and Petrology*, 98, 129–138, https://doi.org/10.1007/BF00402106.

Lindner, M., Finger, F., 2018. Geochemical characteristics of the Late Proterozoic Spitz granodiorite gneiss in the Drosendorf Unit (Southern Bohemian Massif, Austria) and implications for regional tectonic interpretations. *Journal of Geosciences*, 63, 345–362, https://doi.org/10.3190/jgeosci.271.

Lindner, M., Dörr, W., Reither, D., Finger, F., 2020. The Dobra Gneiss and the Drosendorf Unit in the southeastern Bohemian Massif, Austria: West Amazonian crust in the heart of Europe. Murphy, J. B., Strachan, R. A., Quesada, C. (eds). *Geological Society, London, Special Publications*, 503, SP503-2019–2232, https://doi.org/10.1144/SP503-2019-232.

Linnemann, U., Pereira, M.F., Jeffries, T.E., Drost, K., Gerdes, A., 2008. The Cadomian Orogeny and the opening of the Rheic Ocean: The diacrony of geotectonic processes constrained by LA-ICP-MS U-Pb zircon dating (Ossa-Morena and Saxo-Thuringian Zones, Iberian and Bohemian Massifs). *Tectonophysics*, 461, 21–43, https://doi.org/10.1016/j.tecto.2008.05.002.

Linner, M., 1992. *Metamorphose Der Paragneise in Der Monotonen Serie (SE Moldanubikum). Thesis*, 125. University of Vienna.

Matos, R., Teixeira, W., Geraldes, M.C., Bettencourt, J.S., 2009. Geochemistry and Nd-Sr isotopic signatures of the Pensamiento Granitoid Complex, Rondonian-San Ignacio Province, eastern Precambrian shield of Bolivia: Petrogenetic constraints for a Mesoproterozoic magmatic arc setting. *Geologia USP - Serie Cientifica*, 9, 89–117, https://doi.org/10.5327/Z1519-874X2009000200005.

Matos, J.B., Ruiz, A.S., de Sousa, M.Z.A., Batata, M.E.F., Lima, G.A. de, Lafon, J.-M., 2017. Petrologia e Geocronologia U-Pb do Granito Tarumã : Batólito sin-tectônico da Orogenia San Petrologia e Geocronologia U-Pb do Granito Tarumã : Batólito sin-tectônico da Orogenia San Ignácio - Terreno Paraguá , SW do Cráton Amazônico. *Contribuições à Geologia da Amazônia*, 10, 181–194.

Matura, A., 1976. Hypothesen zum Bau und zur geologischen Geschichte des kristallinen Grundgebirges von Südwestmähren und dem niederösterreichischen Waldviertel. *Jahrbuch der Geologischen Bundesanstalt*, 119, 63–75.

Matura, A., 2003. Zur tektonischen Gliederung der variszischen Metamorphite im Waldviertel Niederösterreichs. *Jahrbuch der Geologischen Bundesanstalt*, 143, 221–225.

Mayer, A., Gerdes, A., Janoušek, V., Starijaš Mayer, B., Finger, F., Erban, V., 2013. The Waidhofen Amphibolite Body in the Moldanubian Zone of Lower Austria: a relic of Proterozoic Avalonian crust. *Proceedings of the joint conference of the Czech and German geological societies held in Plzen (Pilsen), September 16 - 19, 2013, Schriftenreihe der Deutschen Gesellschaft für Geowis-senschaften*, 82, 79.

Meschede, M., 2015. *Geologie Deutschlands*, 249. Berlin, Heidelberg, Springer Berlin Heidelberg, https://doi.org/10.1007/978-3-662-45298-1.

Mielke, P., Winkler, H.G.F., 1979. Eine bessere Berechnung der Mesonorm für granitische Gesteine. *Neues Jahrbuch für Mineralogie, Monatshefte*, 471–480.

Nance, R.D., Gutiérrez-Alonso, G., Duncan Keppie, J., Linnemann, U., Murphy, B., Quesada, C., Strachan, R.A., Woodcock, N.H., 2012. A brief history of the Rheic Ocean. *Geoscience Frontiers*, 3, 125–135, https://doi.org/10.1016/j.gsf.2011.11.008.

Neubauer, F., Klötzli, U.S., Poscheschnik, P., 2001. Cadomian magmatism in the Alps recorded in Late Ordovician sandstones of the Carnic Alps: preliminary results from zircon Pb/Pb evaporation dating. *Schweizerische Mineralogische und Petrographische Mitteilungen*, 81, 175–179.

O'Brien, P.J., Carswell, D.A., 1993. Tectonometamorphic evolution of the Bohemian Massif: evidence from high pressure metamorphic rocks. *Geologische Rundschau*, 82, 531–555.

O'Brien, P.J., Vrána, S., 1995. Eclogites with a Short-Lived Granulite-Facies Overprint in the Moldanubian Zone, Czech-Republic - Petrology, Geochemistry and Diffusion Modeling of Garnet Zoning. *Geologische Rundschau*, 84, 473–488.

Otten, M.T., 1984. The origin of brown hornblende in the Artfjället gabbro and dolerites. *Contributions to*

Mineralogy and Petrology, 86, 189–199, https://doi.org/10.1007/BF00381846.

Pearce, J.A., Harris, N.B.W., Tindle, A.G., 1984. Trace element distribution diagrams for the tectonic interpretation of granitic rocks. *Journal of Petrology*, 25, 956–983, https://doi.org/10.1093/petrology/25.4.956.

René, M., Finger, F., 2016. The Blaník Gneiss in the southern Bohemian Massif (Czech Republic): a rare rock composition among the early palaeozoic granites of Variscan Central Europe. *Mineralogy and Petrology*, 110, 503–514, https://doi.org/10.1007/s00710-016-0427-5.

Rieder, M., Cavazzini, G., S. D' yakonov, Yu., Frank-Kamenetskii, V. A., Gottardi, G., Guggenheim, S., Koval', P. V., Müller, G., Neiva, A. M. R., Radoslovich, E. W., Robert, J.-L., Sassi, F. P., Takeda, H., Weiss, Z., Wones, D.R., 1999. Nomenclature of the Micas. *Mineralogical Magazine*, 63, 267–279, https://doi.org/10.1180/002646199548385.

Schantl, P., Hauzenberger, C., Finger, F., Müller, T., Linner, M., 2019. New evidence for the prograde and retrograde PT-path of high-pressure granulites, Moldanubian Zone, Lower Austria, by Zr-in-rutile thermometry and garnet diffusion modelling. *Lithos*, 342–343, 420–439, https://doi.org/10.1016/j.lithos.2019.05.041.

Schuster, R., Daurer, A., Krenmayr, H.G., Linner, M., Mandl, G.W., Pestal, G., Reitner, J.M., 2019. *Rocky Austria: Geologie von Österreich - Kurz Und Bunt*, 80, 5th ed. Wien, Verlag der Geologischen Bundesanstalt.

Scott, J.M., Konrad-Schmolke, M., O'Brien, P.J., Günter, C., 2013. High-T, low-P formation of rare olivine-bearing symplectites in variscan eclogite. *Journal of Petrology*, 54, 1375–1398, https://doi.org/10.1093/petrology/egt015.

Siegesmund, S., Heinrichs, T., Romer, R.L., Doman, D., 2007. Age constraints on the evolution of the Austroalpine basement to the south of the Tauern window. *International Journal of Earth Sciences*, 96, 415–432, https://doi.org/10.1007/s00531-006-0115-5.

Soejono, I., Janoušek, V., Žáčková, E., Sláma, J., Konopásek, J., Machek, M., Hanžl, P., 2017. Long-lasting Cadomian magmatic activity along an active northern Gondwana margin: U–Pb zircon and Sr–Nd isotopic evidence from the Brunovistulian Domain, eastern Bohemian Massif. *International Journal of Earth Sciences*, 106, 2109–2129, https://doi.org/10.1007/s00531-016-1416-y.

Sorger, D., Hauzenberger, C.A., Finger, F., Linner, M., 2020. Two generations of Variscan garnet: Implications from a petrochronological study of a high-grade Avalonia-derived paragneiss from the Drosendorf unit, Bohemian Massif. *Gondwana Research*, 85, 124–148, https://doi.org/10.1016/j.gr.2020.04.004.

Stephan, T., Kroner, U., Romer, R.L., 2019. The pre-orogenic detrital zircon record of the Peri-Gondwanan crust. *Geological Magazine*, 156, 281–307, https://doi.org/10.1017/S0016756818000031.

Streckeisen, A.L., 1974. Classification and nomenclature of plutonic rocks recommendations of the IUGS subcommission on the systematics of Igneous Rocks. *Geologische Rundschau*, 63, 773–786.

Suess, F.E., 1926. *Intrusionstektonik Und Wandertektonik Im Variszischen Grundgebirge*, 268. Berlin, Gebrüder Borntraeger.

Sun, S. -s., McDonough, W.F., 1989. Chemical and isotopic systematics of oceanic basalts: implications for mantle composition and processes. *Geological Society, London, Special Publications*, 42, 313–345, https://doi.org/10.1144/GSL.SP.1989.042.01.19.

Tait, J.A., Bachtadse, V., Franke, W., Soffel, H., 1997. Geodynamic evolution of the European Variscan fold belt: palaeomagnetic and geological constraints. *Geologische Rundschau*, 86, 585-598, https://doi.org/10.1007/s005310050165.

Thiele, O., 1984. Zum Deckenbau und Achsenplan des Moldanubikums der südlichen Böhmischen Masse (Österreich). *Jahrbuch der Geologischen Bundesanstalt*, 126, 513–523.

Vermeesch, P., 2018. IsoplotR: A free and open toolbox for geochronology. *Geoscience Frontiers*, 9, 1479-1493, https://doi.org/10.1016/j.gsf.2018.04.001.

Waldmann, L., 1951. Das außeralpine Grundgebirge Österreichs. *In*: *Schaffer, F. X., Geologie von Österreich, Deuticke, Wien*. 1–105.

Whitney, D.L., Evans, B.W., 2010. Abbreviations for names of rock-forming minerals. *American Mineralogist*, 95, 185–187, https://doi.org/10.2138/am.2010.3371.

Žák, J., Verner, K., Janousek, V., Holub, F.V., Kachlik, V., Finger, F., Hajna, J., Tomek, F., Vondrovic, L., Trubac, J., 2014. A plate-kinematic model for the assembly of the Bohemian Massif constrained by structural relationships around granitoid plutons. *Geological Society, London, Special Publications*, 405, 169–196, https://doi.org/10.1144/SP405.9.

Żelaźniewicz, A., Buła, Z., Fanning, M., Seghedi, A., Zaba, J., 2009. More evidence on Neoproterozoic terranes in Southern Poland and south eastern Romania. *Geological Quarterly*, 53, 93–124.

Żelaźniewicz, A., Oberc-Dziedzic, T., Slama, J., 2020. Baltica and the Cadomian orogen in the Ediacaran–Cambrian: a perspective from SE Poland. *International Journal of Earth Sciences*, https://doi.org/10.1007/s00531-020-01858-0.

Zenk, M., Schulz, B., 2004. Zoned Ca-amphiboles and related P-T evolution in metabasites from the classical Barrovian metamorphic zones in Scotland. *Mineralogical Magazine*, 68, 769–786, https://doi.org/10.1180/0026461046850218.